

# Bose-Einstein correlations in perturbative QCD: $v_n$ dependence on multiplicity.

E. Gotsman<sup>1,\*</sup> and E. Levin<sup>1,2,†</sup>

<sup>1</sup>*Department of Particle Physics, School of Physics and Astronomy,  
Raymond and Beverly Sackler Faculty of Exact Science, Tel Aviv University, Tel Aviv, 69978, Israel*

<sup>2</sup>*Departamento de Física, Universidad Técnica Federico Santa María, and Centro Científico-  
Tecnológico de Valparaíso, Avda. España 1680, Casilla 110-V, Valparaíso, Chile*

(Dated: September 28, 2018)

In this paper we study the dependence of Bose-Einstein correlations on the multiplicity of an event. We found that events with large multiplicity, stem from the production of several parton showers, while the additional production of small multiplicity in the central rapidity region (central diffraction), gives a negligible contribution due to emission of soft gluons, that leads to the Sudakov suppression of the exclusive production of two gluon jets. Hence, the Bose-Einstein correlation is the main source of the azimuthal angle correlations which generates  $v_n$  with odd and even  $n$ . We found, that without this suppression, the measurement of an event with given multiplicity, yields  $v_{n,n} < 0$  for odd  $n$ . It appears that in hadron-nucleus and nucleus-nucleus collisions, the Bose-Einstein correlations do not depend on multiplicity, while for hadron-hadron scattering, such dependence can be considerable. We proposed a simple Kharzeev-Levin-Nardi (KLN) type model, to describe the dependence of azimuthal angle correlations on the centrality of the event, in ion-ion collisions.

PACS numbers: 12.38.-t, 24.85.+p, 25.75.-q

## Contents

<b>I. Introduction</b>	2
<b>II. Symmetry <math>\varphi \rightarrow \pi - \varphi</math> (<math>v_n = 0</math> for odd <math>n</math>) for different multiplicities of produced hadrons</b>	3
A. The Bose-Einstein correlation function for deuteron-deuteron scattering with the correlation length $L_c \propto R_D$	3
B. Bose-Einstein correlation function for heavy ions scattering with the correlation length $L_c \propto R_A$	8
1. Inclusive measurements	8
2. Measurements with fixed multiplicity $N = m\bar{n}$ ,	10
3. Measurements with multiplicity $N \geq m\bar{n}$ ,	11
<b>III. Dependence of Bose-Einstein correlations on the multiplicity of the event</b>	12
<b>IV. A simple KLN -type model for the structure of one parton cascade in CGC</b>	14
A. Momentum dependence of the BFKL Pomeron in a nucleus.	14
B. The model.	17
1. The general formulae.	17
2. The Choice of parameters.	19
3. Comparison with the experimental data.	20
<b>V. Conclusions</b>	20
<b>A. Integration over longitudinal momenta</b>	20
<b>B. Vertices for two gluon production in the central rapidity region</b>	22
<b>References</b>	23

## I. INTRODUCTION

In this paper we continue to discuss the Bose-Einstein correlations of gluons as being the main source of the strong azimuthal angle ( $\varphi$ ) correlations, that have been observed experimentally, in nucleus-nucleus, hadron-nucleus and hadron hadron collisions [1–11]. It has been known for some time in the framework of Gribov Pomeron Calculus, that the Bose-Einstein correlations which stem from the exchange of two Pomerons lead to azimuthal angle correlations[12] (see also Ref.[13]), which do not depend on the rapidity difference between measured hadrons ( large range rapidity (LRR) correlations). In the framework of QCD, these azimuthal correlations originate from the production of two patron showers, and have been re-discovered in Refs.[14–18] (see also Ref.[19, 20]). In Ref.[21] it was demonstrated that Bose-Einstein correlations generate  $v_n$  with even and odd  $n$ , with values which are close to the experimental observed ones.

The goal of this paper is to answer three questions: (i) Is the symmetry  $\varphi \rightarrow \pi - \varphi$  an inherent property of QCD, or of the colour glass condensate (CGC) approach, which is the effective theory of QCD at high energies, or it is based on the model assumptions? (ii) What is the multiplicity dependence of the azimuthal angle correlations which stem from the Bose-Einstein ones? (iii) Is it possible to build a simple KLN-type [22–28] approach to describe azimuthal correlations in nucleus-nucleus collisions?

The following are our answers to these questions: The symmetry  $\varphi \rightarrow \pi - \varphi$ , is not a general feature of the QCD (or CGC) approach. It does not stem from the Bose-Einstein correlations of identical gluons, and can only appear in measurements that mix events with different multiplicities. In the case of hadron-hadron collisions, for example, such symmetry exists in the Born approximation of perturbative QCD, and could only be measured, if experimentally the central diffraction production and the event with double multiplicity ( $n = 2\bar{n}$ , where  $\bar{n}$  is the average multiplicity in inclusive production) are measured and summed. However, the emission of soft gluons for the central exclusive production in the Double Log Approximation of perturbative QCD, leads to a Sudakov form factor which suppress this contribution. Therefore, the Bose-Einstein correlations prevail, leading to  $v_n \neq 0$  for odd  $n$ , even in totally inclusive measurements, without selection of an event with given multiplicities.

We expect a very mild dependence of  $v_n$  on the multiplicity of the observed events. We suggest a model for the Bose-Einstein correlations in heavy ion collisions in the spirit of the KLN approach, which is based on the concept of constructing the simplest model that takes into account the discussed phenomena: in our case, the saturation of the gluon density and the Bose-Einstein correlations.

The double inclusive cross section of two identical gluons has the following general form:

$$\frac{d^2\sigma}{dy_1 dy_2 d^2p_{T1} d^2p_{T2}} (\text{identical gluons}) = \frac{d^2\sigma}{dy_1 dy_2 d^2p_{T1} d^2p_{T2}} (\text{different gluons}) \left( 1 + C(L_c |\mathbf{p}_{T2} - \mathbf{p}_{T1}|) \right) \quad (1)$$

where  $C(L_c |\mathbf{p}_{T2} - \mathbf{p}_{T1}|)$  denotes the correlation function and  $L_c$  the correlation length. Eq. (1) is in accord with Hanbury Brown and Twiss formula (see Refs. [29, 30])

$$\frac{d^2\sigma}{dy_1 dy_2 d^2p_{T1} d^2p_{T2}} (\text{identical gluons}) \propto \left\langle 1 + e^{ir_\mu Q_\mu} \right\rangle \quad (2)$$

where averaging  $\langle \dots \rangle$  includes the integration over  $r_\mu = r_{1,\mu} - r_{2,\mu}$ . There is only one difference:  $Q_\mu = p_{1,\mu} - p_{2,\mu}$  degenerates to  $\mathbf{Q} \equiv \mathbf{p}_{T,12} = \mathbf{p}_{T2} - \mathbf{p}_{T1}$ , as the production of two gluons from the two parton showers, does not depend on rapidities.

Eq. (2) allows us to measure the typical  $r_\mu$  of the interaction, or in other words,  $L_c$  in Eq. (1) is determined by the typical volume of the interaction. Therefore, we expect several typical  $L_c$ : the size of the nucleus  $R_A$ ; the nucleon size  $R_N$  and the typical size, related to the saturation scale ( $r_{\text{sat}} = 1/Q_s$ , where  $Q_s$  denotes the saturation scale[31]). Indication of all these sizes have been seen in Bose - Einstein correlations (see Ref.[17, 21]). Using Eq. (1) we can find  $v_n$ , since

$$\frac{d^2\sigma}{dy_1 dy_2 d^2p_{T1} d^2p_{T2}} \propto 1 + 2 \sum_n v_{n,n}(p_{T1}, p_{T2}) \cos(n\varphi) \quad (3)$$

where  $\varphi$  is the angle between  $\mathbf{p}_{T1}$  and  $\mathbf{p}_{T2}$ .  $v_n$  is determined from  $v_{n,n}(p_{T1}, p_{T2})$

$$1. \ v_n(p_T) = \sqrt{v_{n,n}(p_T, p_T)}; \quad 2. \ v_n(p_T) = \frac{v_{n,n}(p_T, p_T^{\text{Ref}})}{\sqrt{v_{n,n}(p_T^{\text{Ref}}, p_T^{\text{Ref}})}}; \quad (4)$$

Eq. (4)-1 and Eq. (4)-2 depict two methods of how the values of  $v_n$  have been extracted from the experimentally measured  $v_{n,n}(p_{T1}, p_{T2})$ .  $p_T^{\text{Ref}}$  denotes the momentum of the reference trigger. These two definitions are equivalent if  $v_{n,n}(p_{T1}, p_{T2})$  can be factorized as  $v_{n,n}(p_{T1}, p_{T2}) = v_n(p_{T1}) v_n(p_{T2})$ .

## II. SYMMETRY $\varphi \rightarrow \pi - \varphi$ ( $v_n = 0$ FOR ODD $n$ ) FOR DIFFERENT MULTIPLICITIES OF PRODUCED HADRONS

### A. The Bose-Einstein correlation function for deuteron-deuteron scattering with the correlation length $L_c \propto R_D$

First, we consider the simplest diagram in the Born approximation of perturbative QCD, which we have discussed in Ref.[17] (see Fig. 1-a). This diagram describes the interference between two identical gluons in the process of multiparticle production, or in other words, in the processes of the production of two parton showers. In this diagram  $Q_T \propto 1/R_D$  and  $|\mathbf{Q}_T - \mathbf{p}_{12,T}| \propto 1/R_D$ , where  $R_D$  denotes the deuteron radius, which is much larger than the size of the proton,  $R_N$ . Momenta  $k_T$ ,  $l_T$ ,  $p_{1,T}$  and  $p_{2,T}$  in this diagram are of the order of  $1/R_N \gg 1/R_D$  and, therefore, we can neglect  $Q_T$  as well as  $p_{12,T}$  in the diagram. Bearing this in mind, we see that the correlation function  $C(L_c|\mathbf{p}_{12,T}|)$  is equal to

$$C(L_c|\mathbf{p}_{12,T}|) = \frac{1}{N_c^2 - 1} \frac{\int d^2 Q_T G_D(Q_T) G_D(\mathbf{Q}_T - \mathbf{p}_{12,T})}{\int d^2 Q_T G_D(Q_T) G_D(Q_T)} \quad \text{with} \quad G_D(Q_T) = \int d^2 r e^{i\mathbf{r} \cdot \mathbf{Q}_T} |\Psi_D(r)|^2 \quad (5)$$

where  $r$  denotes the distance between the proton and the neutron in the deuteron.

Eq. (5) displays no symmetry with respect to  $\varphi \rightarrow \pi - \varphi$ . However, we can add a different diagram of Fig. 1-b, which describes the central diffraction production of two different gluons in a colourless state<sup>1</sup>. This diagram depends on  $\mathbf{p}_{1,T} + \mathbf{p}_{2,T}$  and generates the correlation function

$$\tilde{C}(L_c|\mathbf{p}_{1,T} + \mathbf{p}_{2,T}|) \propto \frac{1}{N_c^2 - 1} \frac{\int d^2 Q_T G_D(Q_T) G_D(\mathbf{Q}_T - \mathbf{p}_{1,T} - \mathbf{p}_{2,T})}{\int d^2 Q_T G_D(Q_T) G_D(Q_T)} \quad (6)$$

since in this diagram  $Q_T$  and  $\mathbf{Q}_T - \mathbf{p}_{1,T} - \mathbf{p}_{2,T}$  are of the order of  $1/R_D$ , while  $k_T$ ,  $l_T$ ,  $p_{1,T}$  and  $p_{2,T}$  in this diagram are of the order of  $1/R_N \gg 1/R_D$ , therefore, we can neglect  $Q_T$  as well as  $\mathbf{p}_{1,T} + \mathbf{p}_{2,T}$  in the diagram or, in other words, we can put  $\mathbf{p}_{1,T} = -\mathbf{p}_{2,T}$ . After this substitution, both diagrams have the same expressions.

Therefore, if diagrams of Fig. 1-a and Fig. 1-b have the same weight, the sum will have the symmetry with respect to  $\mathbf{p}_{2,T} \rightarrow -\mathbf{p}_{2,T}$ , restoring the symmetry with respect to  $\varphi \rightarrow \pi - \varphi$ . At first sight this is the case, since all integrations over  $k_T$  and  $l_T$  look the same. However, in these two diagrams this is certainly not the case due to different integration with respect to  $k_-$  and  $l_-$  (or  $k^+$  and  $l^+$ ). These integrations generates 1/4 suppression of the diagram of Fig. 1-b with respect to the diagram of Fig. 1-a. It is a well known fact, which for the first time, has been discussed in the AGK paper of Ref.[32], as well as in the most reviews and books that are devoted to the high energy scattering (in particular those, where one of us is an author [31, 33, 34]). For the completeness of presentation we add appendix A in which we discuss this integration.

However, we found it instructive to discuss the contribution of these two diagrams in the framework of the AGK cutting rules, which is the technique that we will use in considering the dependence of the correlation function on multiplicity of produced particles. First, accounting for emission of the gluons with rapidities larger than  $y_1$  and smaller than  $y_2$ , and considering  $\bar{\alpha}_S|y_1 - y_2| \ll 1$ , we can describe the two partonic showers contribution in deuteron-deuteron scattering by the diagrams of Fig. 2-a and Fig. 2-b.

The AGK cutting rules describe the relative contributions of different processes that stem from two BFKL Pomeron [36, 37] exchange. Fig. 3-a describes the elastic scattering, Fig. 3-b the one parton shower production, that is screened by the BFKL Pomeron exchange. Fig. 3-c is the production of two parton showers. The AGK cutting rules state that the cross sections of these three processes are related as 1 : -4 : 2. The sum of these processes is equal to -1, leading to the negative contribution to the total cross section of two Pomeron exchange. These rules have a rather general

---

<sup>1</sup> We are grateful to Alex Kovner and Michael Lublinsky who drew our attention to this diagram, and explained that in their approach [16] this diagram restores the symmetry  $\phi \rightarrow \pi - \phi$ .

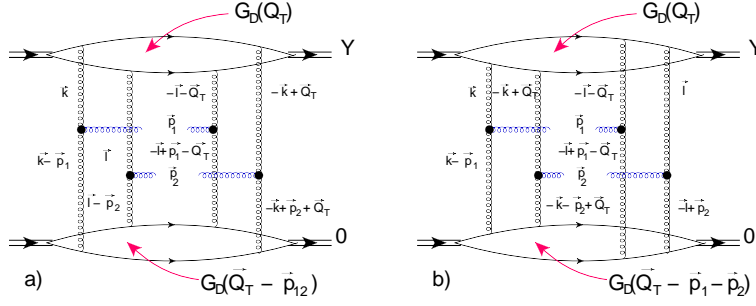


FIG. 1: Deuteron-deuteron scattering in the Born approximation of perturbative QCD: Fig. 1-a describes the interference diagrams in the production of two identical gluons, in the process of multiparticle generation that gives rise to the correlation function  $C(L_c|\mathbf{p}_{12,T} = \mathbf{p}_{1,T} - \mathbf{p}_{2,T})$ ; Fig. 1-b corresponds to the central diffraction of two gluons with different colour charges in the colourless state.

origin based on the unitarity constraints and physical properties of the Pomerons. Indeed, the unitarity constraint has the following form

$$2 \text{Im} A_{el}(s, b; i) = \underbrace{|A_{el}(s, b; i)|^2}_{\text{elastic cross section}} + \underbrace{G(s, b, i)}_{\text{contribution of inelastic processes}} \quad (7)$$

where  $W = \sqrt{s}$  denotes the energy of the collision,  $b$  is impact parameter, and  $i$  the set of other quantum numbers that diagonalize the interaction matrix.

For the BFKL Pomeron, the elastic cross section is much smaller than the exchange of a single Pomeron, and Eq. (7) takes the form

$$2 \text{Im} P^{\text{BFKL}}(s, b, i) = \underbrace{G^{\text{BFKL}}(s, b, i)}_{\text{cut Pomeron}} \quad (8)$$

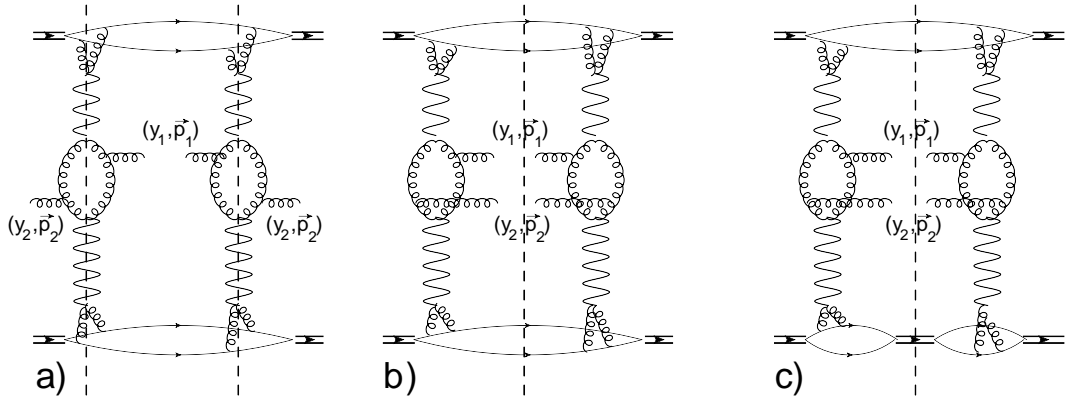


FIG. 2: Mueller diagrams[35] for two parton shower production of gluons: Fig. 2-a describes the interference diagrams in the production of two identical gluons in the process of multiparticle production that generates the correlation function  $C(L_c|\mathbf{p}_{12,T})$ ; Fig. 2-b corresponds to central diffraction of two gluons with different colour charges in the colourless state; Fig. 2-c describes the central diffractive production with a different final state, where one deuteron remains intact. The wavy line stand for the BFKL Pomeron [36]. Helical lines correspond to gluons.

The vertical dashed lines show the cuts.

Using Eq. (8) one can see that

$$\begin{aligned} \sigma_{el} &\propto |P^{\text{BFKL}}(s, b, i)|^2; \quad \sigma_{\text{one parton shower}} \propto -2 P^{\text{BFKL}} G^{\text{BFKL}}(s, b, i); \\ \sigma_{\text{two parton showers}} &\propto -\frac{1}{2} G^{\text{BFKL}}(s, b, i) G^{\text{BFKL}}(s, b, i); \end{aligned} \quad (9)$$

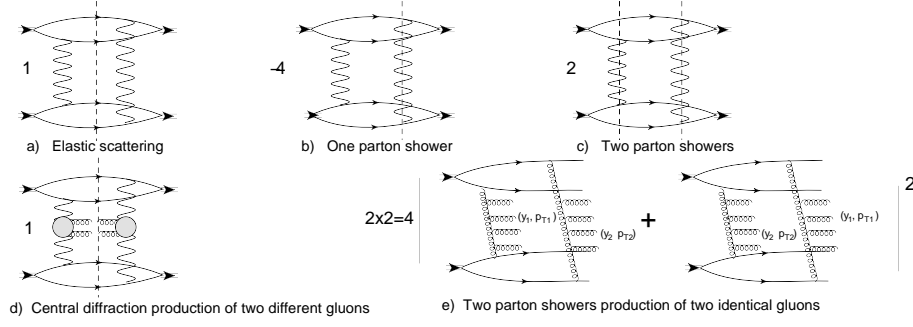


FIG. 3: AGK cutting rules for the exchange of two BFKL Pomeron (Fig. 3(a-c)) and the contributions of the central (Fig. 3-d) and two parton showers production (Fig. 3-e) of two gluons.

where  $\frac{1}{2}$  in the last term stem from the fact that the two cut Pomeron are identical. Using Eq. (8) one reproduces the AGK cutting rules of Fig. 3-a - Fig. 3-c.

The central diffraction production of two gluons is shown in the diagram of Fig. 3-a (elastic scattering), while the interference diagram, that generates the Bose-Einstein correlations, originates from Fig. 3-c with the extra factor 2, which reflects the fact that the gluon with rapidity, say,  $y_1$  can be produced from two different parton cascades (see Fig. 3-e). The processes of central diffractive production are suppressed by a factor of 4 compared to the Bose-Einstein correlations.

To complete the discussion of the possible restoration of  $\varphi \rightarrow \pi - \varphi$  symmetry, due the processes of the central diffraction, we note that in these processes there can be a final state in which one or two deuterons remain intact ( see for example Fig. 2-c) which leads to different correlation functions. For example for Fig. 2-c the correlation function has the form

$$C_{\text{Fig. 2-c}}(L_c|\mathbf{p}_{1,T} + \mathbf{p}_{2,T}) \propto \frac{1}{N_c^2 - 1} \frac{\int d^2 Q_T G_D(Q_T) G_D^2(\mathbf{Q}_T - \mathbf{p}_{1,T} - \mathbf{p}_{2,T})}{\int d^2 Q_T G_D(Q_T) G_D(Q_T)} \quad (10)$$

which differs from Eq. (6).

A comment regarding the status of the AGK cutting rules in QCD. For deuteron-deuteron scattering, the cutting rules shown in Fig. 3-a - Fig. 3-c , have been proved on general grounds[38], using unitarity and the wave nature of the colliding particles. In the framework of perturbative QCD these cutting rules were proven in Refs.[33, 39]. For the inclusive cross sections, the AGK cutting rules were discussed and proven in Refs.[40–46]. However, in Ref.[47] it is shown that the AGK cutting rules are violated for double inclusive production. This violation is intimately related to the enhanced diagrams [46, 47], and reflects the fact that different cuts of the triple BFKL Pomeron vertex lead to different contributions. Recall, that we do not consider such diagrams.

Therefore, the contribution of the central diffraction process is suppressed by a factor of four, due to the longitudinal momenta integration. However, we need to compare the values of the vertices for gluon inclusive production (see Fig. 3-d )and the vertex for two gluon production from the BFKL Pomeron. From Fig. 4 we can see that this vertex, is two times larger than the vertex for gluon inclusive production. Indeed, the contribution of Fig. 4-a is the same as for inclusive production, but we have to add Fig. 4-b. In appendix B we show that these two diagrams (Fig. 4-a and Fig. 4-b) are the same. Adding these diagrams we note that for deuteron-deuteron scattering we expect, the symmetry  $\varphi \rightarrow \pi - \varphi$  in the measurements with no selection on multiplicity. This observation supports the claim of Refs.[15, 16].

In this paper as well as in Refs.[15–17] we discuss the case  $\bar{\alpha}_S|y_1 - y_2| \leq 1$ . Let us consider this restriction more carefully. We start with writing the expression for the two diagrams of Fig. 3-d. The inclusive cross section for production of the gluon with rapidity  $y_1$  and transverse momentum  $p_{1,T}$  due to the exchange of one BFKL Pomeron, has the following form

$$\frac{d\sigma}{dy_1 d^2 p_{T1}} \propto \frac{\bar{\alpha}_S}{p_{1,T}^2} \int d^2 k_T \phi^{\text{BFKL}}(Y - y_1, k_T) \frac{\Gamma_\mu(k_T, p_{1,T}) \Gamma_\mu(k_T, p_{1,T})}{k_T^2 (\mathbf{k}_T - \mathbf{p}_{1,T})^2} \phi^{\text{BFKL}}(y_1, k_T) \quad (11)$$

The interference diagram in which the parton shower with a gluon with  $y_1$  and  $p_{1,T}$  in the amplitude, is squared

with the parton shower in which a gluon with  $y_2$  and  $p_{2,T}$  is produced, takes the form

$$\frac{d\sigma}{dy_1 d^2p_{T1}} \propto \frac{\bar{\alpha}_S}{p_{1,T}^2} \int d^2k_T \phi^{\text{BFKL}}(Y - y_1, k_T) \frac{\Gamma_\mu(k_T, p_{1,T}) \Gamma_\nu(k_T, p_{2,T})}{k_T^2 (\mathbf{k}_T - \mathbf{p}_{2,T})^2} \phi^{\text{BFKL}}(y_2, k_T) \quad (12)$$

In Eq. (11) and Eq. (12) we neglected  $p_{12,T} \propto 1/R_D$  as we have explained above.

In Eq. (11) and Eq. (12)  $\phi$  is the solution of the BFKL equation

$$\frac{\partial \phi^{\text{BFKL}}(y, \mathbf{k}_T)}{\partial y} = \bar{\alpha}_S \int \frac{d^2k'_T}{\pi} \frac{1}{(\mathbf{k}_T - \mathbf{k}'_T)^2} \phi^{\text{BFKL}}(y, \mathbf{k}'_T) - 2\omega_G(\mathbf{k}_T) G(y, \mathbf{k}_T); \quad (13)$$

where

$$\omega_G(\mathbf{k}_T) = \frac{1}{2} \bar{\alpha}_S k_T^2 \int \frac{d^2k'_T}{2\pi} \frac{1}{k'^2_T (\mathbf{k}_T - \mathbf{k}'_T)^2} = \bar{\alpha}_S k_T^2 \int \frac{d^2k'_T}{2\pi} \frac{1}{(k'^2_T + (\mathbf{k}_T - \mathbf{k}'_T)^2) (\mathbf{k}_T - \mathbf{k}'_T)^2} \quad (14)$$

Comparing Eq. (11) and Eq. (12) one can see that to neglect the difference between  $y_2$  and  $y_1$  in  $\phi^{\text{BFKL}}(y_2, k_T)$  we need to assume that  $2.8 \bar{\alpha}_S |y_1 - y_2| \ll 1$  ( $2.8 \bar{\alpha}_S$  is the intercept of the BFKL Pomeron). However, the actual restriction turns out to be even more severe. Indeed, in all interference diagrams as well as in double gluon production between rapidities  $y_1$  and  $y_2$ , we have the exchange in the  $t$ -channel of two gluons in the octet state. This means that we have the additional emission of gluons with rapidities between  $y_1$  and  $y_2$  (see Fig. 4-c). This emission leads to the extra Sudakov form factor[49] in Eq. (12) which takes the form:

$$\frac{d\sigma}{dy_1 d^2p_{T1}} \propto \frac{\bar{\alpha}_S}{p_{1,T}^2} \int d^2k_T e^{-S(\delta y, k_T, p_{1,T})} \phi^{\text{BFKL}}(Y - y_1, k_T) \frac{\Gamma_\mu(k_T, p_{1,T}) \Gamma_\nu(k_T, p_{2,T})}{k_T^2 (\mathbf{k}_T - \mathbf{p}_{2,T})^2} \phi^{\text{BFKL}}(y_2, k_T) \quad (15)$$

where  $\delta Y = |y_1 - y_2|$ . We recall the structure of the one parton shower that is described by the BFKL Pomeron in Fig. 4-e [36], the one parton shower is given by

$$\prod_{i=1}^n \Gamma_\mu(k_{i,T}, p_{i,T}) \frac{e^{\omega_G(k_{i,T})(y_i - y_{i-1})}}{k_{i,T}^2} \quad (16)$$

which being squared, leads to the parton density  $\phi(y, k_{1,T})$ . In simple words the BFKL cascade is the ladder diagram with specific vertices of gluon production, and with the exchange of the reggeized gluons with trajectories which are given by Eq. (14). Absorbing the terms in  $\phi(y, k_T)$  for Eq. (15) we see that

$$S(\delta y, k_T, p_{1,T}) = (\omega(\mathbf{k}_T - \mathbf{p}_{1,T}) + \omega(\mathbf{k}_T)) \delta y = \frac{\bar{\alpha}_S}{2} \left( \ln \left( (\mathbf{k}_T - \mathbf{p}_{1,T})^2 / \mu^2 \right) + \ln(k_T^2 / \mu^2) \right) \delta y \quad (17)$$

and it has a typical Sudakov form factor structure.  $\mu$  is the typical dimensional parameter which in the DGLAP evolution, is of the order of the soft scale in the hadron, and in CGC it is a saturation scale  $Q_s(y_1 \approx y_2)$ .

For the diagrams of Fig. 4-a and Fig. 4-b we need to introduce the same suppressions. These Sudakov suppressions result from the fact that in the approximation for  $\bar{\alpha}_S \delta y \ll 1$  we take into account only simple diagrams with two gluons, and without extra gluon emissions; and they stipulate the size we need to take for  $\delta y$ . However, the two gluon production has an additional suppression of the Sudakov type, which applies even at  $y_1 = y_2$ , where  $S$  of Eq. (17) is equal to zero: the emission of gluons that are shown in Fig. 4-d, has been discussed in detail in Ref.[48, 49].

This emission leads to the value of  $S$  in the double log approximation of perturbative QCD that has the form:

$$S(p_{1,T}, k_T) = \frac{\bar{\alpha}_S}{\pi} \int_{k_T}^{M/2} \frac{d^2q_T}{q_T^2} \int_{q_T}^{M/2} \frac{dq_0}{q_0} = \frac{\bar{\alpha}_S}{4} \ln^2 \left( \frac{M^2}{4k_T^2} \right) \quad (18)$$

where  $M$  denotes the mass of the produced dijet, which is given by  $M^2 = 2p_T^2 (1 + \cosh(y_1 - y_2))$  considering  $\mathbf{p}_{1,T} = -\mathbf{p}_{2,T} = \mathbf{p}_T$ . The limits in integration over  $q_0$  can easily be understood in the rest frame of the two gluon jets. In this frame the minimal  $q_0 = q_T$ . The lower limit in  $q_T$  integration stems from the fact, that at distances less than  $1/q_T$ , the emission with two  $t$ -channel gluons have a destructive interference canceling the emission, since the total colour charge is zero. For  $q_T \geq q_T$  the emission of gluons comes from the  $t$ -channel gluon, which carries color, and leads to the color coefficient in Eq. (18).

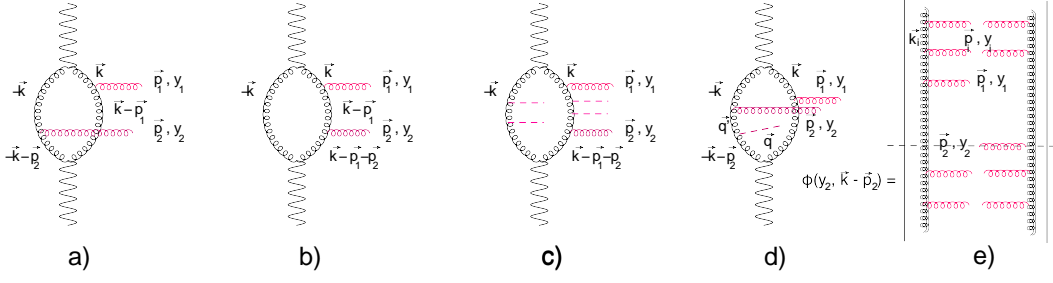


FIG. 4: Vertex for emission of two gluons by the BFKL Pomeron. Fig. 4-c shows the emission of soft gluons whose suppression leads to the Sudakov form factor. Fig. 4 shows the emission of the gluon in the DLA approximation of perturbative QCD, which leads to the Sudakov form factor in the vertex of two gluons emission .

Finally, the contribution of the diagram of Fig. 4-b has the following for  $y_1 = y_2$ :

$$\frac{d\sigma}{dy_1 d^2p_{T1}} (Fig. 4 - b) \propto \frac{\bar{\alpha}_S}{p_{1,T}^2} \int d^2k_T e^{-S(M,k_T)} \phi^{\text{BFKL}}(Y - y_1, k_T) \frac{\Gamma_\mu(k_T, \mathbf{p}_{1,T}) \Gamma_\nu(k_T - \mathbf{p}_{1,T}, \mathbf{p}_{2,T})}{k_T^2 (\mathbf{k}_T - \mathbf{p}_{1,T})^2} \phi^{\text{BFKL}}(y_1, k_T) \quad (19)$$

The integration over  $k_T$  of the parton densities is concentrated in the vicinity of the saturation scale, since in coordinate space  $\phi \propto \nabla^2 N(r, y)$  [50], deep in the saturation region it tends to zero. Of course, we consider not only one BFKL Pomeron, but a more complicated structure of the single parton cascade (see Fig. 5). Therefore, substituting  $Q_s$  instead of  $k_T$  in the Sudakov form factor, we find that Eq. (19) takes the form:

$$\frac{d\sigma}{dy_1 d^2p_{T1}} (Fig. 4 - b) \propto \frac{\bar{\alpha}_S}{p_{1,T}^2} \exp\left(-\frac{\bar{\alpha}_S}{4} \ln^2\left(\frac{p_T^2 (1 + \cosh(y_1 - y_2))}{2 Q_s^2 (y_1 \approx y_2)}\right)\right) \int d^2k_T \phi^{\text{BFKL}}(Y - y_1, k_T) \frac{\Gamma_\mu(k_T, \mathbf{p}_{1,T}) \Gamma_\nu(k_T - \mathbf{p}_{1,T}, \mathbf{p}_{2,T})}{k_T^2 (\mathbf{k}_T - \mathbf{p}_{1,T})^2} \phi^{\text{BFKL}}(y_1, k_T) \quad (20)$$

However, for discussing the current experimental data, especially for hadron-hadron interactions, for the parton densities, we can use the experimental data for DIS structure function which is well described [52], by the DGLAP evolution equations [53]. In this case, we need to put the value of  $Q_0 = Q_s(y_1 = Y_0 \approx 3)$  from the Colour Glass Condensate (CGC) motivated fit of HERA data [54, 55]. This value turns out to be in the range  $Q_0 = 0.2 - 0.5 \text{ GeV}$  [54, 55].

Finally, we obtain the resulting correlation function is the sum of Eq. (6) and Eq. (10):

$$C(\varphi) = C(Eq. (6); L_c 2 p_T \sin(\varphi)) + e^{-\frac{\alpha_S}{2} \ln^2\left(\frac{p_T^2 (1 + \cosh(y_1 - y_2))}{2 Q_s^2}\right)} C(Eq. (10); L_c 2 p_T \cos(\varphi)) \quad (21)$$

where we assume that  $|\mathbf{p}_{1,T}| = |\mathbf{p}_{2,T}| = p_T$ .

The general expectation from Eq. (21) indicates that  $v_n$  with odd  $n$  will peak at  $p_T \approx 4Q_0$ , where the second term will be approximately three times smaller than the first one. The experimental data for  $v_n$  in proton-proton collisions [56] show that  $v_n$  reaches a maximum at  $p_T \approx 3 \text{ GeV}$ , and this value is independent of the energy. Such a behaviour qualitatively supports Eq. (21) with  $Q_0 \approx 0.6 \text{ GeV}$ .

Concluding this section we would like to summarize our results: (i) we showed that at small transverse momenta the processes of exclusive (diffractive) in the central rapidity region (CED) of two gluons, are equal to the interference contributions of two parton showers, confirming the results of Refs. [15, 16], this fact leads to  $v_n = 0$  for odd  $n$ , in the total inclusive measurements, without any selection on multiplicity of produced hadrons; (ii) we found the mechanism of suppression of CED of two gluon jets for large transverse momenta due to Sudakov form factor, which leads to the correlation function of Eq. (6), and to  $v_n \neq 0$  for odd  $n$ , in the experiments without selection on multiplicities; and (iii) only the correlation function of Eq. (5) can be measured in the processes of multiparticle generation with the multiplicities  $N \geq \bar{n}$ , where  $\bar{n}$  is the average multiplicity in the collisions. The process of the central diffraction which generates the correlation function of Eq. (6) corresponds to the event with low multiplicity  $N < \bar{n}$ . The last item is the best motivation for study of the identical particle correlations  $v_n$  with even  $n$ , and with different multiplicities, which we will consider below.

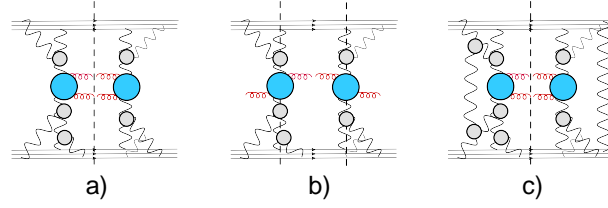


FIG. 5: The double inclusive production for dense-dense parton system scattering: the central diffraction production (see Fig. 5-a) and the Bose-Einstein correlation of the identical gluons ( Fig. 5-b). The wavy lines denote the BFKL Pomerons. Fig. 5-c shows the diagrams that do not contribute for the inclusive production of two gluons. The green blobs show the Mueller vertices for two gluon production, while the circles stand for the triple Pomeron vertices. The produced gluons are denoted by red helical lines.

## B. Bose-Einstein correlation function for heavy ions scattering with the correlation length $L_c \propto R_A$

### 1. Inclusive measurements

Concluding the previous subsection, we claim that for deuteron-deuteron scattering, we see how the processes of the central diffraction, in the measurements that sum processes with all possible multiplicities of produced particles, can lead to the symmetry  $\varphi \rightarrow \pi - \varphi$  for  $p_T \leq Q_s$ . In this section we would like to examine, if such symmetry could be possible for ion-ion interactions, which can be described by the Glauber [57] formula (see Fig. 6-a):

$$A_{AA}(s, b) = i(1 - \exp(-\Omega(s, b))) \quad \text{with} \quad \Omega(s, b) = g_A^2 P^{\text{BFKL}}(s, b) T_{AA}(b) \quad (22)$$

where  $T_{AA}(b)$  is the optical width and given by

$$T_{AA}(b) = \int d^2b' S_A(\mathbf{b} - \mathbf{b}') S_A(\mathbf{b}') \quad \text{with} \quad S_A(b) = \int_{-\infty}^{+\infty} dz \rho(z, \mathbf{b}) \quad \int d^2b S_A(b) = A \quad (23)$$

where  $\rho(z, \mathbf{b})$  denotes the nucleon density in the nucleus, and  $z$  the longitudinal coordinate of the nucleon. In Eq. (22)  $g_N$  denotes the impact factor that describes the interaction of the BFKL Pomeron (whose Green function is  $P^{\text{BFKL}}$ ), with the nucleon.

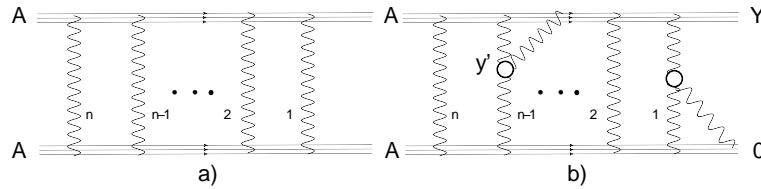


FIG. 6: Nucleus-nucleus scattering in the Glauber[57] approach (Fig. 6-a), and the first corrections to this approach due to triple BFKL Pomeron interactions (Fig. 6-b). The wavy lines denote the BFKL Pomerons. The blobs show the triple Pomeron vertices.

We wish to stress that Eq. (22) in the framework of perturbative QCD (pQCD) has a region of applicability. Indeed, the contribution of one BFKL Pomeron in pQCD, in Eq. (22), is proportional to  $g_N^2 P^{\text{BFKL}} T_{AA}(b) \propto \bar{\alpha}_S^2 A^{4/3} \exp(\Delta_{\text{BFKL}} Y)$  where  $\Delta_{\text{BFKL}} \propto \bar{\alpha}_S$ , where  $\Delta_{\text{BFKL}}$  denotes the BFKL Pomeron intercept. The first ‘fan’ diagrams lead to corrections to the Glauber formula, these are shown in Fig. 6-b, and are of the order

$$g_N^2 P^{\text{BFKL}}(Y) T_{AA}(b) \int_0^Y dy' G_{3P} g_N P^{\text{BFKL}}(y') S_A(b) \propto \bar{\alpha}_S^4 A (P^{\text{BFKL}}(Y, b))^2 \quad (24)$$

Comparing Eq. (24) with the exchange of two BFKL Pomerons, we see that the contribution of the fan diagrams will be smaller than 1 for  $\Delta_{\text{BFKL}} Y \ll \frac{1}{2} \ln(1/(\bar{\alpha}_S^4 A))$ , while the contribution of the BFKL Pomeron in Glauber formula



will be larger than 1. In other words, for  $Y \leq (1/(2\Delta_{\text{BFKL}})) \ln(1/(\bar{\alpha}_S^4 A))$  we can describe the ion-ion collisions using the Glauber formula of Eq. (22).

In this formula the contributions of  $n$ -BFKL Pomeron exchanges to the total cross section is equal to

$$\sigma_{\text{tot}}^{(n)} = \frac{2(-1)^{n-1}}{n!} \Omega^n(s, b). \quad (25)$$

Accordingly to the AGK cutting rules, the relative weight of the process with  $m$  cut Pomerons, ( $n - m + 1$  of them are not cut) is equal

$$\frac{\sigma_n^{(m)}}{\sigma_{\text{tot}}^{(n)}} = (-1)^{n-m} \frac{n!}{m!(n-m)!} 2^{n-1} \quad \text{for } m \geq 1; \quad \frac{\sigma_n^{(0)}}{\sigma_{\text{tot}}^{(n)}} = (-1)^n (2^{n-1} - 1); \quad (26)$$

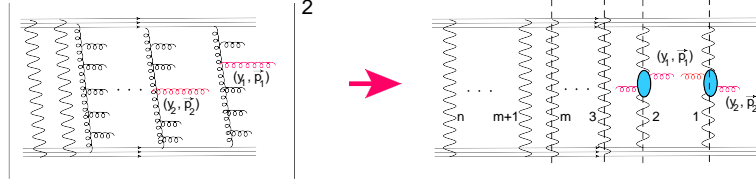


FIG. 7: The contribution of different processes of production of the number of parton showers (more than 2), to the Bose-Einstein correlation. The wavy lines denote the BFKL Pomerons. The blobs show the Mueller vertices for two gluon production. The produced identical gluons are denoted in red helical lines.

To find the contribution of all possible processes of different multiplicities related to the production of  $m$ -parton showers, we need to calculate the following sum (see Fig. 7)

$$\frac{d^2\sigma}{dy_1 dy_2 d^2p_{T1} d^2p_{T2}} = \quad (27)$$

$$C_A(L_c|p_{12,T}|) \frac{d\sigma^{\text{BFKL}}}{dy_1 d^2p_{T1}} \frac{d\sigma^{\text{BFKL}}}{dy_2 d^2p_{T2}} \sum_{m=2}^{\infty} \sum_{n=m}^{\infty} m(m-1) \frac{\sigma_n^{(m)}}{\Omega^2(s, b)} = 4C(L_c|p_{12,T}|) \frac{d\sigma^{\text{BFKL}}}{dy_1 d^2p_{T1}} \frac{d\sigma^{\text{BFKL}}}{dy_2 d^2p_{T2}}$$

In Eq. (27) we use Eq. (26), Eq. (25), the function  $C_A$  is determined by an equation which is similar to Eq. (5). Neglecting all correlations inside the nucleus, its wave function can be written as  $\Psi_A(\{r_i\}) = \prod_{i=1}^A \Psi_i(r_i)$  where  $\Psi(r_i)$  denotes the wave function of  $i$ -th nucleon. In this approach

$$C_A(L_c|p_{12,T}|) = \frac{1}{N_c^2 - 1} \frac{\int d^2Q_T G_A^2(Q_T) G_A^2(\mathbf{Q}_T - \mathbf{p}_{12,T})}{\int d^2Q_T G_A^4(Q_T)} \quad \text{with} \quad G_A(Q_T) = \int d^2b e^{i\mathbf{b} \cdot \mathbf{Q}_T} S_A(b) \quad (28)$$

where  $S_A(b)$  denotes the number of the nucleons at fixed impact parameter  $b$ .

Eq. (28) can be re-written in the impact parameter representation using Eq. (23): viz.

$$C_A(L_c|p_{12,T}|) = \frac{1}{N_c^2 - 1} \frac{\int d^2\tilde{b} e^{i\tilde{b} \cdot \mathbf{p}_{12,T}} T_A^2(\tilde{b})}{\int d^2\tilde{b} T_A^2(\tilde{b})} \quad \text{where} \quad T_A(b) = \int d^2b' S_A(b') S_A(\mathbf{b} - \mathbf{b}') \quad (29)$$

The production of gluons by the BFKL Pomerons given by the Mueller diagrams in Fig. 7, generally has a more complicated form than we used in Eq. (27) (see Eq.(38) of Ref.[17]), and cannot be reduced to the production of single inclusive cross sections. However, in the case of deuteron scattering, we can consider  $\mathbf{p}_{1,T} = \mathbf{p}_{2,T}$ , since the difference  $p_{12,T} \sim 1/R_D \ll 1/R_N$  or  $\ll Q_s$ , where  $1/R_N$  and  $Q_s$  are typical momenta in the BFKL Pomeron. Bearing this in mind, we can replace the contribution of the Mueller diagram by the single inclusive production of the gluon, by the BFKL Pomeron.

The contribution to the central diffraction productions is shown in Fig. 8, and takes the following form

$$\begin{aligned} \frac{d^2\sigma}{dy_1 dy_2 d^2p_{T1} d^2p_{T2}} &= \\ C_A(L_c|\mathbf{p}_{1,T} + \mathbf{p}_{2,T}|) &\frac{d\sigma^{\text{BFKL}}}{dy_1 d^2p_{T1}} \frac{d\sigma^{\text{BFKL}}}{dy_2 d^2p_{T2}} \left( \sum_2^{n-2} \frac{n!}{2!(n-2)!} \frac{\sigma_n^{(0)}}{\Omega^2(s,b)} + \sum_{n=1}^{\infty} \sum_{m=1}^{n-2} \frac{n!}{2!(n-m-2)!} \frac{\sigma_n^{(m)}}{\Omega^2(s,b)} \right) \\ &= C_A(L_c|\mathbf{p}_{1,T} + \mathbf{p}_{2,T}|) \frac{d\sigma^{\text{BFKL}}}{dy_1 d^2p_{T1}} \frac{d\sigma^{\text{BFKL}}}{dy_2 d^2p_{T2}} \xrightarrow{\Omega \gg 1} 2 C_A(L_c|\mathbf{p}_{1,T} + \mathbf{p}_{2,T}|) \frac{d\sigma^{\text{BFKL}}}{dy_1 d^2p_{T1}} \frac{d\sigma^{\text{BFKL}}}{dy_2 d^2p_{T2}} \end{aligned} \quad (30)$$

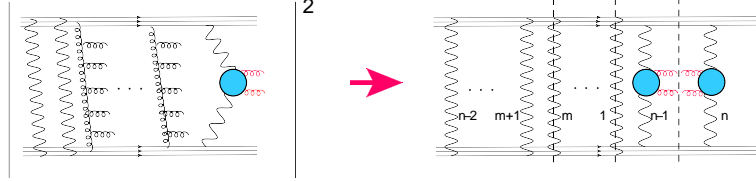


FIG. 8: The contribution of different processes of production of the number of parton showers to the central diffraction production. The wavy lines denote the BFKL Pomerons. The blobs show the Mueller vertices for two gluons production. The produced gluons are denoted by red helical lines.

In Eq. (30) we use Eq. (26), Eq. (25) and the function  $C_A(L_c|\mathbf{p}_{1,T} + \mathbf{p}_{2,T}|)$  from Eq. (29), as well as  $\mathbf{p}_{1,T} = -\mathbf{p}_{1,2}$  for deuteron-deuteron scattering. Actually, these estimates are correct only in the region of large  $\Omega$ . The general expression for the correlation function has the following form

$$\begin{aligned} C_A(L_c|\mathbf{p}_{1,T} + \mathbf{p}_{2,T}|) &= \\ \frac{1}{N_c^2 - 1} &\frac{\int d^2\tilde{b} e^{i\tilde{b} \cdot (\mathbf{p}_{1,T} + \mathbf{p}_{2,T})} \int d^2B \int d^2b S_A\left(\mathbf{B} + \frac{1}{2}\tilde{b}\right) S_A\left(\mathbf{B} - \frac{1}{2}\tilde{b}\right) S_A\left(\mathbf{b} + \frac{1}{2}\tilde{b}\right) S_A\left(\mathbf{b} - \frac{1}{2}\tilde{b}\right) \left(2 - \exp(-\Omega(\mathbf{b} + \mathbf{B}))\right)}{\int d^2\tilde{b} \int d^2B \int d^2b S_A\left(\mathbf{B} + \frac{1}{2}\tilde{b}\right) S_A\left(\mathbf{B} - \frac{1}{2}\tilde{b}\right) S_A\left(\mathbf{b} + \frac{1}{2}\tilde{b}\right) S_A\left(\mathbf{b} - \frac{1}{2}\tilde{b}\right) \left(2 - \exp(-\Omega(\mathbf{b} + \mathbf{B}))\right)} \end{aligned} \quad (31)$$

We also make use of the fact that the Mueller vertex for production of two gluons by the BFKL Pomeron (see Fig. 8), is equal to the Mueller vertex for inclusive production of a single gluon (see Fig. 7).

Comparing Eq. (27) and Eq. (30) we see that the contribution of the central diffraction production, is twice as large (at small  $p_T$ ) than the contribution of the Bose-Einstein correlations. Therefore, the dominant contribution comes from Eq. (30) leading to the negative values of  $v_{n,n}$  for odd  $n$ . This prediction contradicts experimental observations. Such a situation could result for two reasons: (1) the measured  $p_T$  are larger than typical momentum  $Q_0$ , and this contribution is suppressed, as has been discussed in Eq. (21); and (2) the measurements were not made in an inclusive type of the experiment, in which all events were summed without selection on multiplicities of the secondary hadron, but only events with large multiplicity were measured.

## 2. Measurements with fixed multiplicity $\mathbf{N} = m\bar{n}$ ,

First, we would like to examine what happens to the symmetry  $\varphi \rightarrow \pi - \varphi$  in an event with given multiplicity. We need to compare the production of  $m$  parton showers which generate the event with multiplicity  $N = m\bar{n}$ , with the event with the same multiplicity, but in which we produce in addition the low multiplicity events, by central diffraction production. From the point of view of the AGK cutting rules, the first process, is the process with  $m$ -cut Pomerons, while the second, is the process with the same  $m$ -cut Pomerons, plus two Pomerons which are not cut. At first sight, the second case could have a larger cross section, since it has an additional factor  $(\sigma_{\text{in}} T_A(b))^2$ , which can be large for nucleus-nucleus scattering. We need to estimate this contribution since it is suppressed by factor  $\exp(-2\Omega)$  in Eq. (39). In Fig. 9 we plot the  $b$ -dependence of  $\sigma^{(m)}(b)$  of Eq. (39), together with the coefficient from the AGK cutting rules. From this figure we see that the processes of central diffraction in the inelastic environment

is dominant, except for the process with  $N = 2\bar{n}$  which needs additional consideration. This fact is a bit surprising since

$$\begin{aligned} \text{Inelastic production: } N = m\bar{n} \quad \sigma_{in}^{(m)} &\propto \frac{m(m-1)}{m!} (2\Omega(b))^{m-2} \exp(-2\Omega(b)); \\ \text{Inelastic production + CED: } N = m\bar{n} \quad \sigma_{CED}^{(m)} &\propto \frac{2}{m!} (2\Omega(b))^m \exp(-2\Omega(b)); \end{aligned} \quad (32)$$

The survival probability  $\exp(-2\Omega(b))$ , is very small at all  $b$  less than  $2R_A$ , and determines the value for  $2\Omega(b) \leq 1$ . Therefore, the extra factor  $(2\Omega)^2$ , is not an enhancement, but a suppression (see Fig. 9-c). Nevertheless, it turns out that together with numerical coefficients this kind of suppression does not work.

However, we need to consider the contribution to the correlation function, which includes the additional integrations over impact parameters,

$$\begin{aligned} C(\mathbf{p}_{1,T} \pm \mathbf{p}_{2,T}) &= \int d^2\tilde{b} e^{(\mathbf{p}_{1,T} \pm \mathbf{p}_{2,T}) \cdot \tilde{\mathbf{b}}} \tilde{c}(\tilde{\mathbf{b}}); & \tilde{c}(\tilde{\mathbf{b}}) &= \int d^2B c(\tilde{\mathbf{b}}, \mathbf{B}) \\ c(\tilde{\mathbf{b}}, \mathbf{B}) &= \int d^2b S_A\left(\mathbf{B} + \frac{1}{2}\tilde{\mathbf{b}}\right) S_A\left(\mathbf{B} - \frac{1}{2}\tilde{\mathbf{b}}\right) S_A\left(\mathbf{b} + \frac{1}{2}\tilde{\mathbf{b}}\right) S_A\left(\mathbf{b} - \frac{1}{2}\tilde{\mathbf{b}}\right) \sigma_{in,CED}^{(m)}(\mathbf{B}) \end{aligned} \quad (33)$$

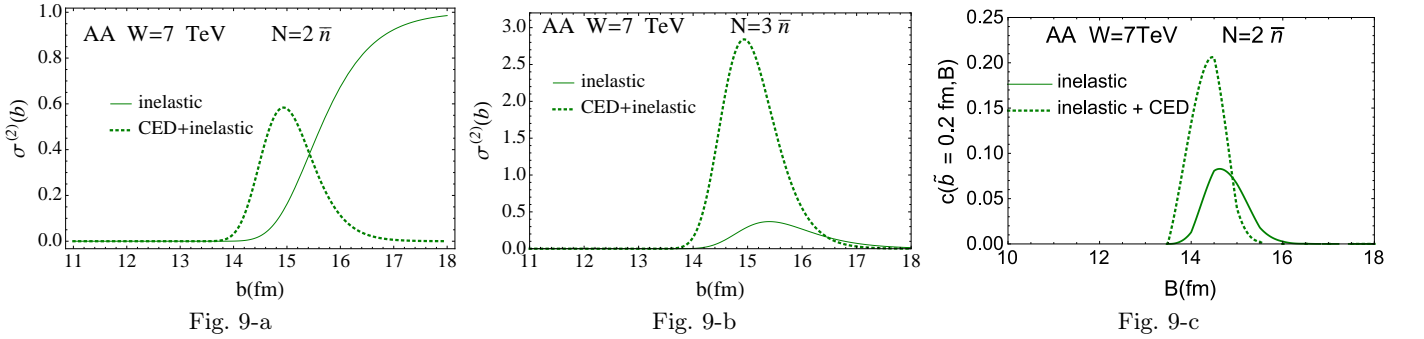


FIG. 9: Comparison of the inelastic events with the multiplicity  $N = m\bar{n}$ : for the production of two identical gluons from the  $m$ -parton showers, and central diffraction production in the event: Fig. 9-a for  $m=2$  and Fig. 9-b for  $m=3$ . Fig. 9-c shows the same contribution as Fig. 9-a after all integrations. .

Integration over all impact parameters shows that in the event with  $N = 2\bar{n}$ , the process with dijet production is also larger than the Bose-Einstein correlations (see Fig. 9-c).

One can see that the multiparticle production accompanied by exclusive production of two gluon jet prevails, leading to negative  $v_{n,n}$ , for odd  $n$ . For nucleus-nucleus collisions, it is well known, that this statement contradicts the experimental data [6, 7, 11].

### 3. Measurements with multiplicity $N \geq m\bar{n}$ ,

Hence, for nucleus-nucleus scattering, the inclusive experiments, as well as the measurements with fixed multiplicity in the Leading  $\text{Log}(1/x)$  Approximation of perturbative QCD, generate negative  $v_{n,n}$  for odd  $n$ , which contradicts the experimental data. In this subsection we examine the situation when the events with multiplicities larger that  $m_0\bar{n}$  ( $N \geq m_0\bar{n}$ ) is measured, as it has been done in the most experiments. Summing Eq. (32) over all  $m \geq m_0$  we obtain

$$\sigma_{in}^{m_0}(Y; B) = 1 - \frac{\Gamma(m_0 - 2, 2\Omega(B; Y))}{\Gamma(m_0 - 2)} \xrightarrow{\Omega \gg 1} 1 - \frac{(2\Omega(B; Y))^{m_0-3}}{(m_0 - 3)!} e^{-2\Omega(B; Y)}; \quad (34)$$

$$\sigma_{CED}^{m_0}(Y; B) = 2\left(1 - \frac{\Gamma(m_0, 2\Omega(B; Y))}{\Gamma(m_0)}\right) \xrightarrow{\Omega \gg 1} 2\left(1 - \frac{(2\Omega(B; Y))^{m_0-1}}{(m_0 - 1)!} e^{-2\Omega(B; Y)}\right); \quad (35)$$

One can see that at large  $\Omega$ , that the inelastic event with additional dijet production, is larger than the inelastic event that generates the Bose-Einstein correlations. In Fig. 10-a we plot the function  $\tilde{c}(\tilde{b})$  of Eq. (33), which also

shows that the inelastic contribution with dijet production prevails. Fig. 10-b shows the correlation functions of Eq. (6) and Eq. (10). Note that the Bose-Einstein correlations are smaller than the correlations due to the diffractive production of dijets.

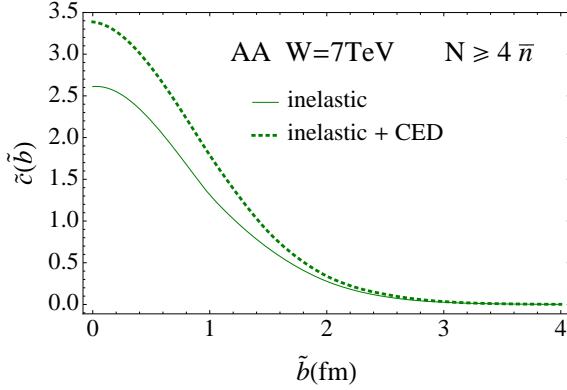


Fig. 10-a

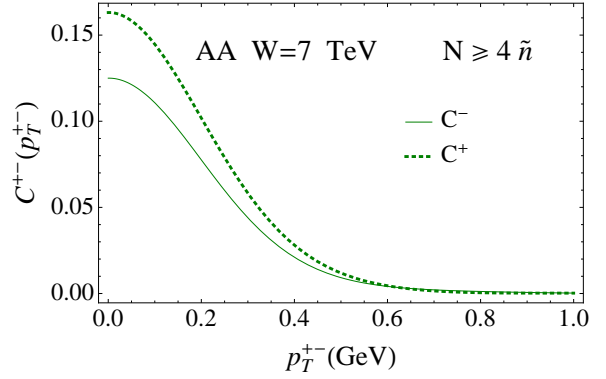


Fig. 10-b

FIG. 10: Comparison of the inelastic events with the multiplicity  $N \geq m_0 \bar{n}$  in gold-gold collision at  $W = 7 \text{ TeV}$ : for the production of two identical gluons for larger than  $m_0$ -parton showers, and central diffraction production in the event with the multiplicity not smaller than  $m_0 \bar{n}$ . Fig. 10-a shows the contribution of inelastic event and inelastic even plus central diffraction, for  $m_0 = 4$ . In Fig. 10-b we plot the correlation functions  $C^\pm(|\mathbf{p}_{1,T} \pm \mathbf{p}_{2,T}|)$  (see Eq. (6) and Eq. (10)).  $p_T^\pm \equiv |\mathbf{p}_{1,T} \pm \mathbf{p}_{2,T}|$ .

Hence, the experimental results are in direct contradiction with the theoretical predictions based on the Leading  $\text{Log}(1/x)$  Approximation of perturbative QCD. The only explanation that we can suggest is, that the Sudakov form factor suppresses the dijets production.

We believe that the  $p$  measured  $p_T$  turns out to be much larger than  $Q_0$ , and double log suppression results in a small contribution of the process of central diffraction. Indeed, for the exchange of the BFKL Pomeron our value for  $Q_0 \approx Q_s(y_1)$  appears to be overestimated. Our conclusions that typical  $k_T \approx Q_s$  is based on the diagrams of Fig. 5-a and Fig. 5-b, in which the same diagrams contribute to central diffraction and the inclusive cross section. However, for the exclusive central production there no AGK cutting rules, and the diagrams of Fig. 5-c should be taken into account. If we remove the integral in Eq. (19) for the Sudakov form factor, the remaining expression takes the form of Eq. (20). For the BFKL Pomeron, it is just the contribution to the total cross section. The typical transverse momenta in the BFKL Pomeron, both increase and decrease as function of rapidity (see Ref[58]) and at large  $y_2$  or  $Y - y_1$ , the typical  $k_T$  is as small as the non-perturbative soft momentum, which could be of the order of  $\Lambda_{\text{QCD}}$ . If we replace the emission of gluons by Eq. (20), the diagrams of Fig.5-c reduce to the contribution to the total cross section, supporting the idea that  $Q_0$  is of the order of typical soft momentum. Therefore, we expect that  $Q_0 \approx \mu_{\text{soft}} \approx \Lambda_{\text{QCD}}$ . Bearing this in mind we concentrate our efforts below on the calculating Bose-Einstein correlations, and their dependence on multiplicity of the events.

### III. DEPENDENCE OF BOSE-EINSTEIN CORRELATIONS ON THE MULTIPLICITY OF THE EVENT

In this section, we consider the dependence of Bose-Einstein correlations on the multiplicity of the event, using the Glauber formula for the total cross section. In accord with the AGK cutting rules, the multiplicity of the event ( $N$ ) is intimately related to the number of parton showers ( $m$ ) that are produced, where  $N = m \bar{n}$ .

In the framework of this approach, the Bose-Einstein correlations in the event with multiplicity  $N = m \bar{n}$  is

determined by the following expression (see also Eq. (33)):

$$\frac{d^2\sigma}{dy_1 dy_2 d^2p_{T1} d^2p_{T2}} \propto C_A(L_c|\mathbf{p}_{12,T}|) \frac{d\sigma^{\text{BFKL}}}{dy_1 d^2p_{T1}} \frac{d\sigma^{\text{BFKL}}}{dy_2 d^2p_{T2}}; \quad (36)$$

$$C_A(L_c|\mathbf{p}_{12,T}|) = \frac{1}{N_c^2 - 1} \frac{I(L_c|\mathbf{p}_{12,T}|)}{I(0)}, \quad I(L_c|\mathbf{p}_{12,T}|) = \int d^2\tilde{b} e^{i\tilde{\mathbf{b}} \cdot \mathbf{p}_{12,T}} \mathcal{I}(\tilde{b}) \quad (37)$$

$$\mathcal{I}(\tilde{b}) = \int d^2B c(\tilde{b}, \mathbf{B}) \quad (38)$$

$$\sigma^{(m)}(\mathbf{B} + \mathbf{b}) = \sum_{n=m, m \geq 2}^{\infty} m(m-1) \frac{\sigma_n^{(m)}}{\Omega^2(s, \mathbf{B})} = \frac{(2\Omega(s, \mathbf{B}))^{m-2}}{(m-2)!} e^{-2\Omega(s, \mathbf{B})} \quad (39)$$

If we assume  $S_A(b)$  to have a Gaussian form i.e.  $S_A(b) = (A/(\pi R_A^2)) \exp(-b^2/R_A^2)$ , then Eq. (38) takes the form

$$\mathcal{I}(\tilde{b}) = \left( \frac{A}{\pi R_A^2} \right)^4 e^{-\frac{\tilde{b}^2}{R_A^2}} \left( \int d^2B d^2b e^{-2\frac{(B^2+b^2)}{R_A^2}} \frac{\sigma_n^{(m)}(\mathbf{B} + \mathbf{b})}{\Omega^2(s, \mathbf{B} + \mathbf{b})} \right) \quad (40)$$

and the correlation function does not depend on  $m$  or, in other words, it does not depend on the multiplicity of the event. However, this result is the specific property of the Gaussian approximation, which cannot be correct even for hadron-hadron collisions, since it does not lead to the correct exponential behaviour of the scattering amplitude at large impact parameters  $b$ . Considering the Glauber model for the description of the proton-proton scattering at high energies, we replace  $S_A$  and  $T_A$  in Eq. (28) and Eq. (29) by

$$S_N(b) = \frac{m^2}{2\pi} K_0(mb); \quad T_N = \int d^2b' S_N(b') S_N(\mathbf{b} - \mathbf{b}'); \quad \Omega = \sigma_0 e^{\Delta Y} T_N(b) \quad (41)$$

where  $\sigma_0 = 41/\text{GeV}^2$ ,  $m = 1 \text{ GeV}$  and  $\Delta = 0.1$ , were chosen to describe the value and energy behaviour of the total cross section for the proton-proton interaction at high energy. In Fig. 11-a the behaviour of  $\mathcal{I}(b)$  is shown for the events with different multiplicities. We see that the correlation length  $L_c$  decreases as function of the multiplicity. In other words, the typical momentum in the correlation function  $C(L_c p_{12,T})$  increases with  $N$ , as can be seen from Fig. 11-b, where the value of the correlation function  $C(L_c p_{12,T})$  is plotted.

The correlation length of the correlation function in nucleus-nucleus collisions, shows only mild dependence on the multiplicity of the events, (see Fig. 12-b, while the value of  $\mathcal{I}$  crucially depends on  $N$  (see Fig. 12-a). Fig. 12-c shows that the correlation function  $C_A(L_c p_{12,T})$  does not depend on the multiplicity of the event.

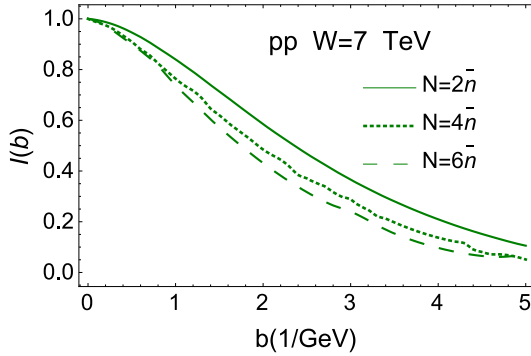


Fig. 11-a

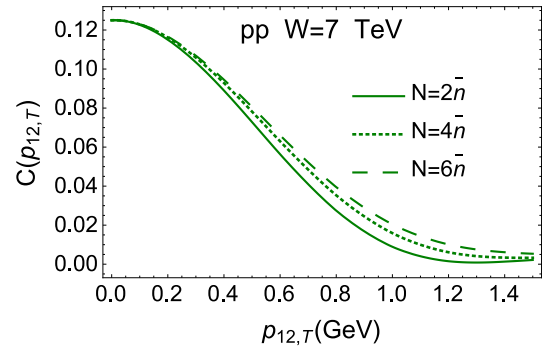


Fig. 11-b

FIG. 11: Fig. 11-a shows  $\mathcal{I}(b)$  for proton-proton scattering with the parameters, that are given in Eq. (41), as a function of  $b$ , for the events with different multiplicities normalized to 1 at  $b = 0$ . In Fig. 11-b the correlation function  $C(p_{12,T})$  is plotted versus  $p_{12,T}$ .  $\bar{n}$  is the average multiplicity in the single inclusive production.

For completeness of presentation we calculated both  $\mathcal{I}(b)$  and  $C_{pA}(p_{12,T})$  for proton-gold scattering.

The results of these calculations are plotted in Fig. 13. The first observation is that the correlation length does not depend on the size of the nucleus, and is determined by the typical impact parameter in proton-proton scattering. The dependence on multiplicity of the event is rather mild.

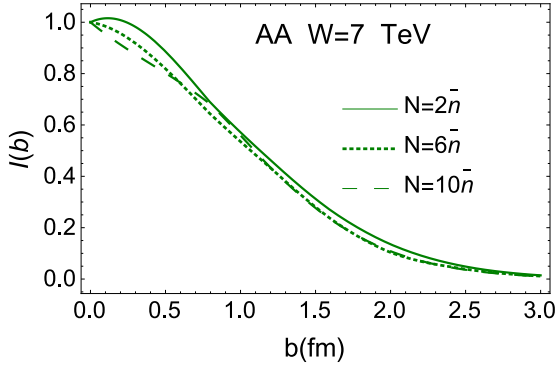


Fig. 12-a

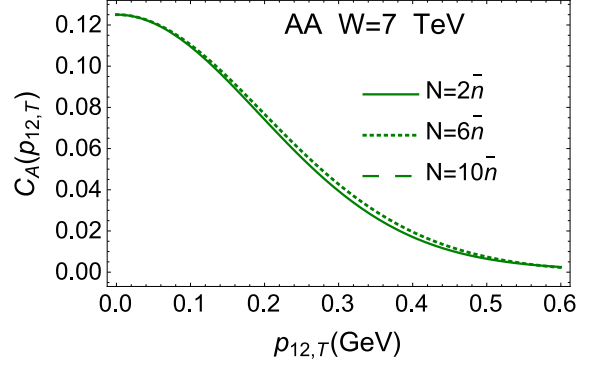


Fig. 12-b

FIG. 12:  $\mathcal{I}(b)$  for nucleus-nucleus (gold-gold) scattering with  $S_A(b)$  given in Eq. (28), as a function of  $b$ , for the events with different multiplicities. In Fig. 12-a  $\mathcal{I}(b)$  are normalized to their values at  $b = 0$ .  $\bar{n}$  is the average multiplicity in the single inclusive production. The correlation function  $C(p_{212,T})$  is plotted in Fig. 12-b.

Concluding this section, we would like to emphasize that the dependence on multiplicity due to the production of several parton showers, turns out to be mild, except for the case of hadron-hadron collisions. For this collision the larger multiplicity of the event, the shorter is the correlation length  $L_c$ , or, in other words, the typical momentum increases in the events with large multiplicities. On the other hand, such an increase is not very pronounced, and even for hadron-hadron collisions, we can expect that the main source of the multiplicity dependence is from the structure of one parton shower. In the next section, we discuss the saturation of the parton density in the one parton shower for nucleus-nucleus collisions, and we develop a simple model in the spirit of the KLN approach.

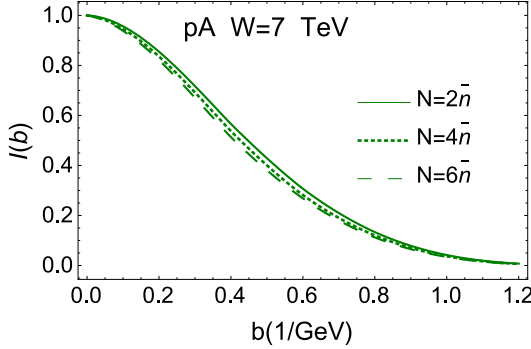


Fig. 13-a

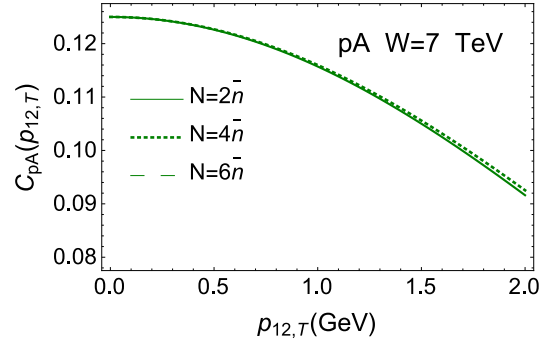


Fig. 13-b

FIG. 13: Fig. 13-a shows  $\mathcal{I}(b)$  for proton-gold scattering with the parameters that are given in Eq. (28), and with the typical  $b = 1 \text{ 1/GeV}$  in proton-proton scattering, as a function of  $b$ , for the events with different multiplicities, normalized to 1 at  $b = 0$ . In Fig. 13-b the correlation function  $C_{pA}(p_{12,T})$  is plotted versus  $p_{12,T}$ .  $\bar{n}$  denotes the average multiplicity in single inclusive production.

#### IV. A SIMPLE KLN -TYPE MODEL FOR THE STRUCTURE OF ONE PARTON CASCADE IN CGC

##### A. Momentum dependence of the BFKL Pomeron in a nucleus.

As we have seen, the diagrams in which the structure of the one parton shower is described by the BFKL Pomeron, lead to the correlation length of azimuthal angle correlations  $L_c \propto 1/R_A$  or, in other words, to the typical transverse momentum which is very small (see Fig. 12). Therefore, we need to discuss a more complicated structure of the single parton shower, which is related, for example, to ‘fan’ diagrams shown in Fig. 5-b. We expect that the interaction of the BFKL Pomeron will lead to the value of  $L_c \sim 1/Q_{s,A}$ , where  $Q_{s,A}$  denotes the nucleus saturation momentum. In particular, we consider the diagrams of Fig. 14-a and Fig. 14-b. The diagram of Fig. 14-a is the first diagram that

leads to the correlation function which depends on the saturation momentum of the nucleon, as shown in Ref.[17, 21]. We will show that the interaction of the BFKL Pomeron with the nucleus, examples of which are shown in Fig. 14-b, will lead to  $L_c \propto 1/Q_{s,A}$ .

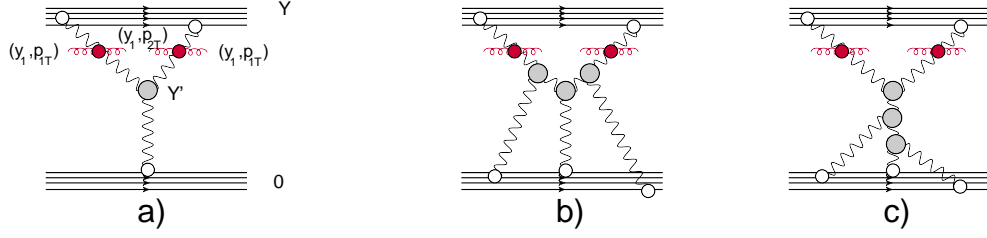


FIG. 14: The double inclusive production for ion-ion collisions which lead to the azimuthal correlations with the correlation length  $L_c \propto 1/Q_s$ : the first diagram is displayed in Fig. 14-a, while Fig. 14-b shows the interaction of the BFKL Pomeron which results in  $L_c \propto 1/Q_{s,A}$ , where  $Q_{s,A}$  denotes the saturation momentum of the nucleus. The wavy lines denote the BFKL Pomeron. The red blobs show the Mueller vertices for two gluons production, while the gray circles stand for the triple Pomeron vertices. The white circles show the vertex of the interaction of the BFKL Pomeron with the nucleus. The produced gluons are denoted by red helical lines. For simplicity we draw the diagrams at  $y_1 = y_2$ .

The general equation for the propagator of the BFKL Pomeron in a nucleus is shown in Fig. 15. The simplest form these equation have in the framework of Gribov Pomeron Calculus [59] with  $\alpha'_P = 0$  and the Pomeron intercept  $\Delta$ . Denoting by  $T_A(Y, Q_T; Y'Q'_T)$  and  $G_A(Y, Q_T)$  the dressed (resulting) propagator of the Pomeron, and the solution

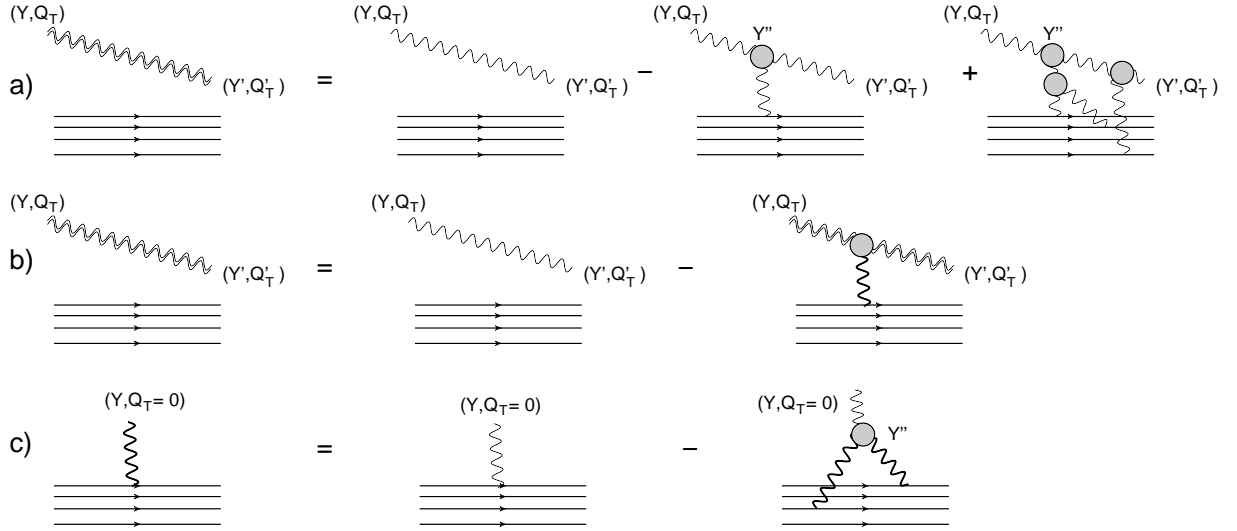


FIG. 15: Equations for BFKL Pomeron propagator in the nucleus. Fig. 15-a shows the first simple diagrams. Fig. 15-b presents the equation for the propagator. Fig. 15-c describes the Balitsky-Kovchegov equation. Wavy lines describes the BFKL Pomeron. The double wavy lines denote the resulting propagator. The bold wavy lines stand for the solution of Balitsky-Kovchegov equation in the nucleus. The blobs denote the triple Pomeron vertices.

of the non-linear Balitsky-Kovchegov equation of Fig. 15-c, respectively, the equations take the forms

$$T_A(Y, Q_T; Y'Q'_T) = T(Y - Y', Q_T) - \Delta \int_0^Y dY'' d^2 Q''_T T(Y - Y'', Q_T) G_A(Y'', Q_T - Q''_T) T_A(Y'', Q''_T; Y'Q'_T); \quad (42)$$

$$\frac{\partial T_A(Y, Q_T; Y'Q'_T)}{\partial Y} = \Delta \left( T_A(Y, Q_T; Y'Q'_T) - \int d^2 Q''_T G_A(Y, Q_T - Q''_T) T_A(Y, Q''_T; Y'Q'_T) \right); \quad (43)$$

$$T(Y - Y', Q_T) = g(Q_T) \exp(\Delta(Y - Y')); \quad T_A(Y = Y', Q_T; Y'Q'_T) = g(Q_T); \quad (44)$$

$$G_A(Y, Q_T) = G(Y - Y', Q_T) - \Delta \int_0^Y dY'' d^2 Q_T'' G^0(Y - Y'', Q_T) G_A(Y'', Q_T - Q_T'') G_A(Y'', Q_T''; Y' Q_T'); \quad (45)$$

$$\frac{\partial G_A(Y, Q_T)}{\partial Y} = \Delta \left( G_A(Y, Q_T) - \int d^2 Q_T'' G_A(Y, Q_T - Q_T'') G_A(Y, Q_T'') \right); \quad (46)$$

$$G^0(Y - Y', Q_T) = \exp(\Delta(Y - Y')); \quad G_A(Y = 0, Q_T) = S_A(Q_T) \quad \text{with} \quad S_A(Q_T) = \int d^2 b e^{i Q_T \cdot b} S_A(b); \quad (47)$$

The main idea of solution, is the observation that in  $G_A(Y, Q_T)$  the typical  $Q_T \sim 1/R_A \ll 1/R_N$  or  $Q_s$ , where  $R_N$  is the nucleon size. Therefore, in Eq. (42)-Eq. (47) we can replace  $G_A(Y, Q_T)$  by  $\int d^2 Q_T G_A(Y, Q_T) \delta^2(Q_T)$ . At  $Y = 0$ ,  $\int d^2 Q_T G_A(Y, Q_T) = S_A(b = 0) \propto 2\rho R_A$ , where  $\rho$  denotes the density of the nucleons in a nucleus. Plugging this expression in the above equations, they reduce to the following form

$$\frac{dT_A(Y, Q_T; Y' Q_T')}{dY} = \Delta \left( T_A(Y, Q_T; Y' Q_T') - \tilde{G}_A(Y) T_A(Y, Q_T; Y' Q_T') \right); \quad (48)$$

$$\frac{d\tilde{G}_A(Y)}{dY} = \Delta \left( \tilde{G}_A(Y) - \tilde{G}_A^2(Y) \right) \quad \text{where} \quad \tilde{G}_A(Y) = \int d^2 Q_T G_A(Y, Q_T) \quad (49)$$

Solving Eq. (49) and Eq. (48) we obtain

$$\tilde{G}_A(Y) = \frac{S_A(b = 0) e^{\Delta Y}}{1 + S_A(b = 0) (e^{\Delta Y} - 1)}; \quad T_A(Y, Q_T; Y' Q_T') = g(Q_T) e^{\Delta(Y - Y')} \frac{1 + S_A(b = 0) (e^{\Delta Y'} - 1)}{1 + S_A(b = 0) (e^{\Delta Y} - 1)}; \quad (50)$$

In the general case, the equations have a more complicated structure, and include the dependence on the transverse momenta, which are the Fourier images of the dipole sizes. However, in the vicinity of the saturation scale, the scattering amplitude displays a geometric scaling behaviour[60], and depends only on one variable  $Q_s^2/p_T^2$ . In the vicinity of the saturation scale the equations take the form:

$$\frac{dT_A(z; z')}{dY} = (1 - \gamma_{cr}) \left( T_A(z, z') - \tilde{G}_A(z) T_A(z, z') \right); \quad (51)$$

$$\frac{d\tilde{G}_A(z)}{dz} = (1 - \gamma_{cr}) \left( \tilde{G}_A(z) - \tilde{G}_A^2(z) \right) \quad (52)$$

Solutions of these equations have the following form:

$$\tilde{G}_A(z) = \frac{\phi_0 e^{(1 - \gamma_{cr})z}}{1 + \phi_0 (e^{(1 - \gamma_{cr})z} - 1)}; \quad T_A(z, z') = g(Q_T) e^{(1 - \gamma_{cr})(z - z')} \frac{1 + \phi_0 (e^{(1 - \gamma_{cr})z'} - 1)}{1 + \phi_0 (e^{(1 - \gamma_{cr})z} - 1)}; \quad (53)$$

where  $\phi_0$  denotes the value of the scattering amplitude at  $z = 0$  and

$$z = \ln \left( \frac{Q_{s,A}^2(Y)}{p_T^2} \right) \quad \text{with} \quad Q_{s,A}^2(Y) = S_A(b = 0) Q_s^2(Y) \quad (54)$$

where  $Q_s(Y)$  denotes the proton saturation momentum.

The principle feature of all these solutions is that, the interaction with nucleus, which is shown in Fig. 14-b and in Fig. 15, does not affect the dependence on  $Q_T$ , which determines the angular correlations. The only diagrams that could depend on the nuclear saturation momentum, are shown in Fig. 14-c. Generally speaking the BFKL Pomeron from the rapidity 0 to rapidity  $Y'$ , should be replaced by the dressed BFKL Pomeron (see Fig. 16).





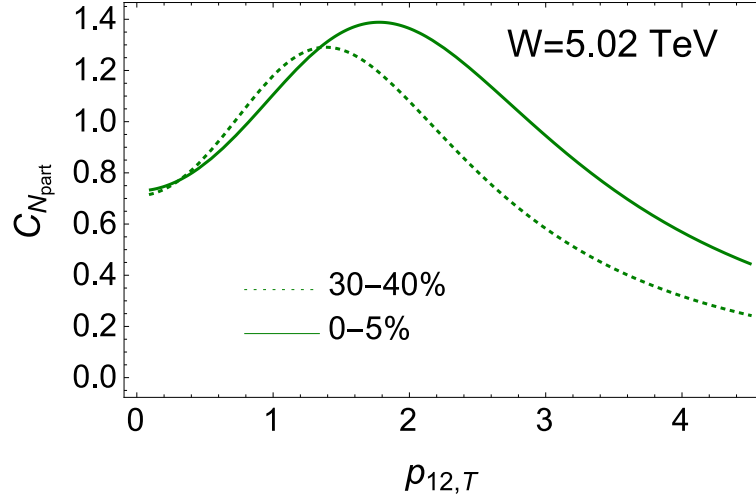


FIG. 17: The correlation function  $C_{N_{part}}(p_{12,T})$  at different centralities: 0-5% and 30-40% , versus  $p_{12,T}$

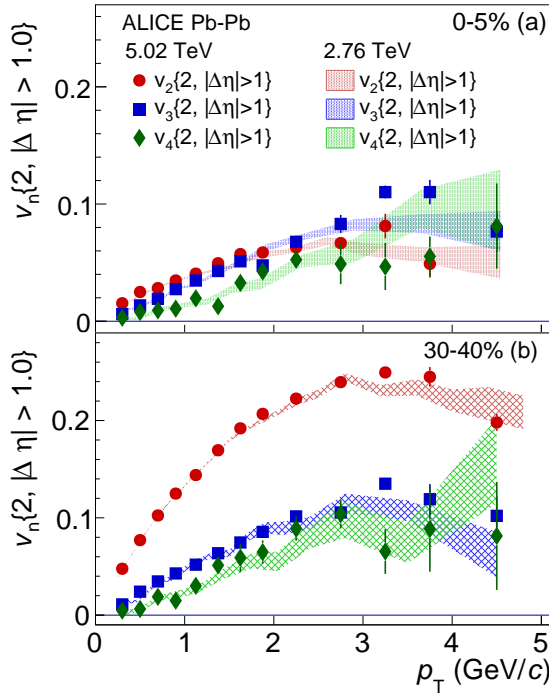


FIG. 18: Experimental data for  $v_n$  versus  $p_T$  [7] at two different centralities: 0-5% in the upper figure and 30-40% in the lower one.

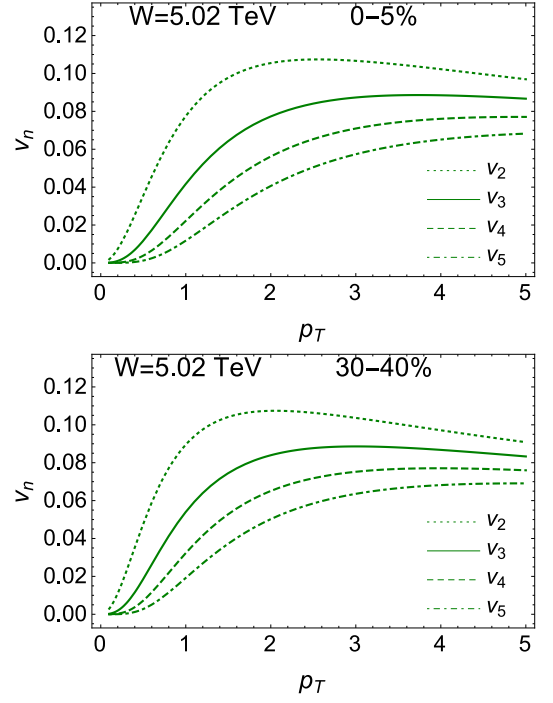


FIG. 19: Our model for  $v_n$  versus  $p_T$  for different centralities: 0-5% in the upper and 30-40% in the lower figures.

The triple Pomeron vertex has been calculated in Ref.[17], and at large  $Q_T$  it has the form (see Eq.(45) and Eq.(A12))

$$\Gamma_{3P}(Q_T, Q_{s,A}) \xrightarrow{Q_T \gg Q_{s,A}} \left( \frac{1}{(k_T - \frac{1}{2}Q_T)^{2\gamma_{cr}} (Q_T^2)^{1-2\gamma_{cr}}} \right)^2 \xrightarrow{Q_T \gg k_T \approx Q_{s,A}} \frac{1}{(Q_T^2)^{2(1-\gamma_{cr})}} \quad (59)$$

where  $k_T$  denotes the momentum inside of the triple Pomeron vertex, which is of the order of the typical saturation momentum of the lower BFKL Pomeron in Fig. 16. To specify dependence of the triple Pomeron vertex, we recall

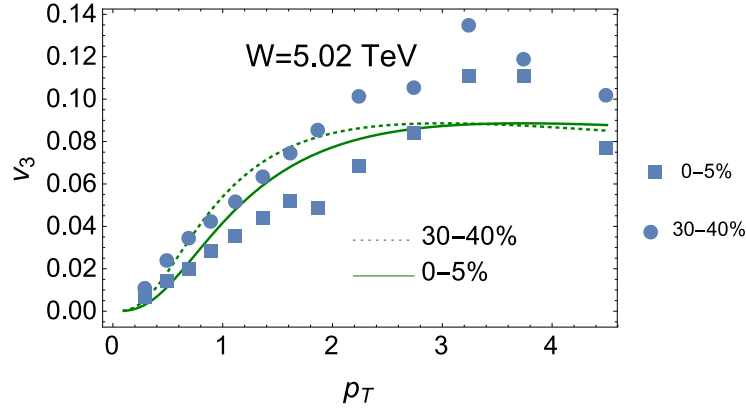


FIG. 20: Comparison of the estimates from our model for  $v_3$ , with the experimental data of ALICE collaboration[7].

that at large impact parameters, the scattering amplitude should decrease exponentially[61]. Bearing this in mind we suggest that

$$\Gamma_{3P}(Q_T, Q_{s,A}) = \left( \frac{Q_s^2}{Q_T^2 + Q_s^2} \right)^{2(1-\gamma_{cr})} \quad (60)$$

which reproduces Eq. (59) at large  $Q_T$ , and has the exponential decrease at large  $b$ .

Plugging Eq. (60) into Eq. (58) we obtain the correlation function in the form

$$C_A(p_{12,T}) = \frac{1}{N_c^2 - 1} \frac{\left( \frac{(1-\phi_0)}{1-\gamma_{cr}} \Gamma_{3P}(Q_T = p_{12,T}, Q_{s,A}(Y_0)) + \phi_0 z_1 \Gamma_{3P}(Q_T = p_{12,T}, \bar{Q}_{s,A}(y_1 \approx y_2)) \right)}{\left( \frac{(1-\phi_0)}{1-\gamma_{cr}} \Gamma_{3P}(Q_T = 0, Q_{s,A}(Y_0)) + \phi_0 z_1 \Gamma_{3P}(Q_T = 0, \bar{Q}_{s,A}(y_1 \approx y_2)) \right)} \quad (61)$$

The multiplicity dependence stems from Eq. (61), where we replace  $Q_{s,A}$  by the value of the saturation momentum, which corresponds to the given number of participants, this in the spirit of the KLN approach[27, 28]. In Fig. 17 the correlation functions are shown for  $W = 5.02$  TeV, and for the choice  $Y_0 = \ln(W_0/m)$  with  $W = 130$  GeV and  $m = 1$  GeV. This function has an essential dependence on  $N_{\text{part}}$ , or on centrality.

$v_n$  can be calculated for  $|p_{1,T}| = |p_{2,T}|$  as

$$v_n = \left( \int d\varphi \cos(n\varphi) C_{N_{\text{part}}}(2p_T \sin(\varphi/2)) \right) / \left( 2\pi + \int d\varphi C_{N_{\text{part}}}(2p_T \sin(\varphi/2)) \right)^{\frac{1}{2}} \quad (62)$$

## 2. The Choice of parameters.

The formulae of Eq. (61) and Eq. (62) depend only on the value of the saturation momentum, and consequently, it depends on rapidity, and  $N_{\text{part}}$ . We follow the KLN-approach[23, 26, 27] in finding these dependences. We assume that

$$Q_s^2(Y; N_{\text{part}}) = \frac{\rho_{\text{part}}}{2} Q_0^2 e^{\lambda(Y-Y_0)}; \quad (63)$$

The value of  $Q_0$  we fix from the gold-gold scattering at  $W = 130$  GeV and for centrality 0 – 5%  $Q_s^2(Y = Y_0) = 2.02$  GeV<sup>2</sup>.  $Y = \ln(W/W_0)$  and  $Y - Y_0 = \ln(W/130)$ .  $\rho_{\text{part}}$  have been calculated in Ref.[23] for the LHC energies, and in Ref.[27] for  $W_0 = 130$  GeV. The choice  $Y_0 = \ln(W_0/m)$  in Eq. (61) is not theoretically determined, note that the value of typical  $\Delta Y'$  in the integral over  $Y'$ , is about  $\Delta Y \sim 1/\bar{\alpha}_S$ , and for  $\bar{\alpha}_S = 0.2$ , this results in a value which is close to the chosen  $Y_0$ . Finally, we take  $\lambda = 0.25$  as it is done in Refs.[23–27].

### 3. Comparison with the experimental data.

Using the parameters, discussed above, we evaluate the correlation function (see Fig. 17, and the values of  $v_n$  which are plotted in Fig. 18, Fig. 19 and Fig. 20). First, we note that the correlation function depends strongly on the centrality, leading to a correlation length which increases for large centralities.

However,  $v_n$  show only mild dependence on centralities (compare Fig. 18 and Fig. 19). Such a behaviour at first sight is in disaccord with the experimental data.  $v_2$  turns out to be smaller than the experimental values for both centralities. On the other hand, the value for  $v_2$ , as well as for other even  $n$ , is not very decisive, since in QCD there are many other sources of  $v_n$  with even  $n$ , beside Bose-Einstein correlations. However, we have not found the other sources for  $v_n$  with even  $n$ . Fig. 20 presents our estimate for  $v_3$  together with the experimental data. We see that our predictions for  $v_3$  describe the experimental data fairly well. Not extremely well, but the model that we develop here, is very simple. These estimates encourage us to develop a more complete description of  $v_n$  for even  $n$ , with different multiplicities, based on the Bose-Einstein correlations.

## V. CONCLUSIONS

We summarize the main results of this paper. The main goal of this paper is to investigate the dependence of Bose-Einstein correlations on the multiplicity of the events. We view these correlations as the major source of the azimuthal angle correlations, and the only known origin of  $v_n$  with odd  $n$  in the framework of the Color Glass Condensate. Indeed, the correlation of identical gluons produces the correlation function that depends on  $|\mathbf{p}_{1,T} - \mathbf{p}_{2,T}|$  which gives  $v_n$  with odd  $n$ . However, in Refs.[15, 16] it was noted, that the diffractive central production of two different gluons in the colorless state leads to dependence on  $|\mathbf{p}_{1,T} + \mathbf{p}_{2,T}|$ . If these two sources have the same strength, the totally inclusive experiments without any selection on multiplicities, will give  $v_n = 0$  for odd  $n$ . In this paper, we showed in the Leading Log(1/x) Approximation of perturbative QCD, the amplitude of two gluon exclusive production turns out to be equal to the interference diagram, that is the source of the Bose-Einstein correlation, in accord with Refs.[15, 16]. However, the emission of soft gluons for the central exclusive production in the Double Log Approximation of perturbative QCD, leads to the Sudakov form factor which suppress this contribution. Therefore, the Bose-Einstein correlations prevail leading to  $v_n \neq 0$  for odd  $n$ . It should be stressed, that without this suppression, the measurement of an event with given multiplicity, yields  $v_{n,n} < 0$  for odd  $n$ .

We demonstrated that the Bose-Einstein correlation function does not depend on the number of produced parton showers for hadron-nucleus and nucleus-nucleus collisions, but for hadron-hadron collisions such dependence turns out to be considerable.

Finally, we developed a simple KLN-type model to describe the Bose-Einstein correlation in one parton cascade, as a function of centralities. The predicted dependence reflects the main features of the observed data, reproduces the value of  $v_n$  with odd  $n$ , but, much work is still needed to develop a more complete approach. This paper encourages us to search for such an approach.

We view this paper as an argument that the description of  $v_n$  is possible due to interactions in the initial state, and that these interactions should not be neglected.

**Acknowledgements** We thank our colleagues at Tel Aviv University and UTFSM for encouraging discussions. Our special thanks go to Carlos Cantreras, Alex Kovner and Michael Lublinsky for elucidating discussions on the subject of this paper.

This research was supported by the BSF grant 2012124, by Proyecto Basal FB 0821(Chile), Fondecyt (Chile) grant 1140842, and by CONICYT grant PIA ACT1406.

## Appendix A: Integration over longitudinal momenta

In this appendix we recall the calculation that results in Eq. (8). For simplicity we restrict ourselves to calculate both the scattering amplitude at high energies ( Pomeron, see Fig. 21-a and Fig. 21-b) and the contribution of the inelastic processes (cut Pomeron,  $G(s)$  in Eq. (8), see Fig. 21-c), in the Born approximation of pQCD.  $G(s, t = 0)$

takes the following form (see Fig. 21-c)

$$\begin{aligned}
G(s, t=0) &= g^4 \mathcal{C} 4s^2 \int \frac{dk^+ dk_- d^2 k_T}{(2\pi i)^4 i} \frac{1}{(k^+ k_- - k_T^2 - i\epsilon)^2} 2\pi \delta((P_1 - k)^2) 2\pi \delta((P_2 + k)^2) \\
&= 16 \mathcal{C} \alpha_S^2 s^2 \int dk^+ dk_- d^2 k_T \frac{1}{(k^+ k_- - k_T^2 - i\epsilon)^2} \delta(-P_1^+ k_- - k_T^2) \delta(P_{2,-} k^+ - k_T^2) \\
&= 16 \mathcal{C} \alpha_S^2 s \int \frac{d^2 k_T}{k_T^4}
\end{aligned} \tag{A1}$$

In Eq. (A1)  $\mathcal{C}$  is the colour coefficient which is the same for all diagrams, factor  $4s^2$  ( $s = (P_1 + P_2)^2 = 2P_{1,\mu} P_2^\mu$  at high energy) stems from the summation over polarization of the  $t$ -channel gluon of the gluon current of quarks  $2P_{1,\mu}$  ( $2P_{2,\mu}$ ).  $\alpha_S = g^2/4\pi$ . Integrating the  $\delta$ -functions, one can see that  $k^+ k_- \ll k_T^2$ .

The scattering amplitude is equal to

$$\begin{aligned}
A(s, t=0) &= g^4 \mathcal{C} 4s^2 \int \frac{dk^+ dk_- d^2 k_T}{(2\pi i)^4 i} \frac{1}{(k^+ k_- - k_T^2 - i\epsilon)^2} \frac{1}{-P_1^+ k_- - k_T^2 - i\epsilon} \\
&\times \left( \underbrace{\frac{1}{P_{2,-} k^+ - k_T^2 - i\epsilon}}_{\text{Fig. 21-a}} + \underbrace{\frac{1}{-P_{2,-} k^+ - k_T^2 - i\epsilon}}_{\text{Fig. 21-b}} \right)
\end{aligned} \tag{A2}$$

For  $k^+ > 0$  we can take the integral over the pole:  $k_-^0 = \frac{-k_T^2 - i\epsilon}{P_1^+}$  closing around this pole, the contour of integration in lower semi-plane in complex  $k_-$  plane, since the integral over large circle decreases at large  $k_-$ . The other pole  $k_-^1 = \frac{k_T^2 + i\epsilon}{k^+}$  is located in the upper semi-plane. For  $k^+ < 0$  all singularities are situated in lower semi-plane leading to vanishing of the integral. Bearing this in mind we reduce Eq. (A2) to the following expression:

$$\begin{aligned}
A(s, t=0) &= \frac{8\alpha_S^2}{\pi} \mathcal{C} s^2 \int_0^\infty dk^+ d^2 k_T \frac{1}{k_T^4} \frac{1}{(-P_1^+)} \left( \frac{1}{P_{2,-} k^+ - k_T^2 - i\epsilon} + \frac{1}{-P_{2,-} k^+ - k_T^2 - i\epsilon} \right) \\
&= \frac{8\alpha_S^2}{\pi} \mathcal{C} s^2 \int_{-\infty}^\infty dk^+ d^2 k_T \frac{1}{k_T^4} \frac{1}{(-P_1^+)} \frac{1}{P_{2,-} k^+ - k_T^2 - i\epsilon}
\end{aligned} \tag{A3}$$

Taking the integral over  $k^+$  using contour  $C$  in Fig. 21-d, and taking into account that the integral over a large circle is equal to  $i\pi$  we obtain

$$A(s, t=0) = i 8 \alpha_S^2 \mathcal{C} s \int \frac{d^2 k_T}{k_T^4} \tag{A4}$$

The diagram Fig. 21-c gives the same contribution as the imaginary part of diagram of Fig. 21-a, multiplied by factor 2, since in this diagram we have  $2\pi \delta(P_{2,-} k^+ - k_T^2)$ . Therefore, we obtain that  $2 \text{Im} A(s, t=0) = G(\text{Fig. 21-c})$  which proves Eq. (8) in Born approximation of pQCD.

For the amplitude of the two gluon production (see Fig. 22-a and Fig. 22-b) as well as for the cross section of the one gluon production which is shown in Fig. 22-c, we have the following hierarchy of the longitudinal momenta:

$$P_1^+ \gg p_1^+ \sim p_2^+ \gg k^+; \quad P_{2,-} \gg p_{1,-} \sim p_{2,-} \gg k_-; \tag{A5}$$

assuming that both gluons are produced with almost equal rapidities ( $y_1 \approx y_2$ ) in the central rapidity region ( $y_1 \approx y_2 \ll 1$ ) in c.m.f.

Using Eq. (A5) we can reduce the amplitude to the following expression:

$$\begin{aligned}
A(\text{Fig. 22-a} + \text{Fig. 22-b}) &= \\
&32 \pi \alpha_S^3 \mathcal{C} s^2 \int_0^\infty dk^+ d^2 k_T \frac{1}{k_T^4} \frac{\Gamma_\mu(p_{2,T}, k_T)}{(\mathbf{p}_{2,T} + \mathbf{k}_T)^2} \frac{\Gamma_\nu(p_{1,T}, k_T)}{(\mathbf{p}_{1,T} - \mathbf{k}_T)^2} \frac{1}{(-P_1^+)} \left( \frac{1}{P_{2,-} k^+ - k_T^2 - i\epsilon} + \frac{1}{-P_{2,-} k^+ - k_T^2 - i\epsilon} \right) \\
&= 32 \alpha_S^3 \mathcal{C} s^2 \int_{-\infty}^\infty dk^+ d^2 k_T \frac{1}{k_T^4} \frac{\Gamma_\mu(p_{2,T}, k_T)}{(\mathbf{p}_{2,T} + \mathbf{k}_T)^2} \frac{\Gamma_\nu(p_{1,T}, k_T)}{(\mathbf{p}_{1,T} - \mathbf{k}_T)^2} \frac{1}{(-P_1^+)} \frac{1}{P_{2,-} k^+ - k_T^2 - i\epsilon} \\
&= 32 \pi i \alpha_S^3 \mathcal{C} s \int \frac{\Gamma_\mu(p_{2,T}, k_T)}{k_T^4} \frac{\Gamma_\nu(p_{1,T}, k_T)}{(\mathbf{p}_{2,T} + \mathbf{k}_T)^2} \frac{d^2 k_T}{(\mathbf{p}_{1,T} - \mathbf{k}_T)^2}
\end{aligned} \tag{A6}$$

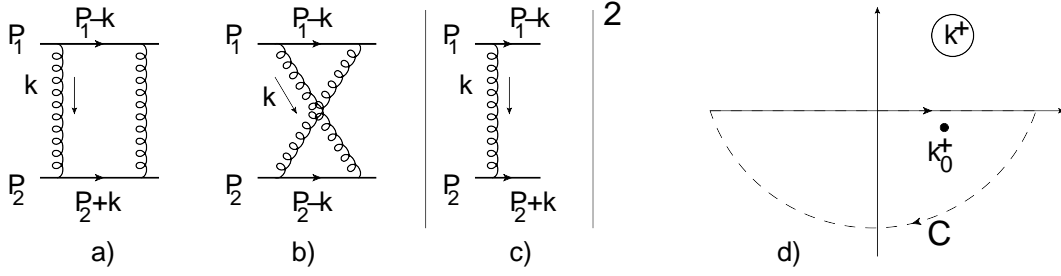


FIG. 21: Born Approximation of pQCD: longitudinal momenta integration. Fig. 21-a and Fig. 21-b are the diagrams for the scattering amplitude at high energy in the  $\bar{\alpha}_S^2$  order of pQCD. Fig. 21-c is the cross section for two quarks production (cut Pomeron). Fig. 21-d shows the contour of integration over  $k^+$ . Helical lines denote gluons, the solid lines indicate quarks.

In Eq. (A6) we use the same contour of integration over  $k^+$  (see Fig. 21-d) as calculating the elastic amplitude (see Eq. (A3)). The Lipatov vertices  $\Gamma_\mu$  for the gluon emission depend only on transverse momenta, and do not influence the integration over longitudinal momenta.

The cross section of Fig. 22-c differs from the amplitude by factor 2, which has the same origin as has been discussed above (see Eq. (A1)).

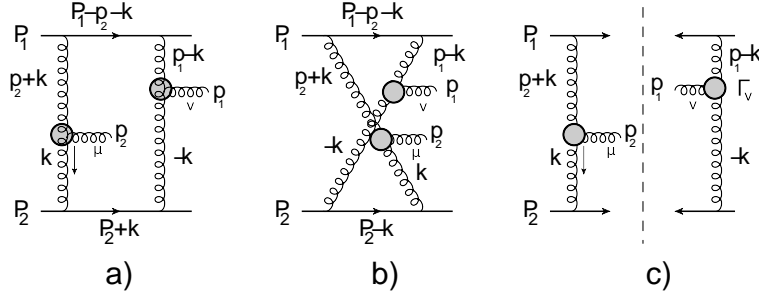


FIG. 22: Born Approximation of pQCD: longitudinal momenta integration. Fig. 22-a and Fig. 22-b are the diagrams for the amplitude for the production of two gluons with momenta  $p_1$  and  $p_2$ , in  $\bar{\alpha}_S^3$  order of pQCD. Fig. 22-c is the cross section for two quarks and two gluons production (cut Pomeron). Helical lines denote gluons, the solid lines indicate quarks. The blobs denote the Lipatov vertices for gluon production ( $\Gamma_\nu$ ).

## Appendix B: Vertices for two gluon production in the central rapidity region

In this appendix we clarify why diagrams Fig. 4-a and Fig. 4-b are equal. The vertex in the diagram of Fig. 4-a has the form

$$V(\text{Fig. 4-a}) = \frac{\Gamma_\mu(k_T, p_{1,T}) \Gamma_\nu(-k_T, p_{2,T})}{k_T^2 (k_T - p_{2,T})^2} \quad (\text{B1})$$

while for Fig. 4-b it can be written as

$$V(\text{Fig. 4-b}) = \frac{\Gamma_\mu(k_T, p_{1,T}) \Gamma_\nu(k_T - p_{1,T}, p_{2,T})}{k_T^2 (k_T - p_{2,T})^2} \quad (\text{B2})$$

We need to calculate these vertices for  $p_{1,T} = -p_{2,T}$ , since  $|p_{1,T} + p_{2,T}| \propto 1/R_D \ll 1/R_N$ .

The vertices  $\Gamma_\mu$  has the following expressions:

$$\Gamma_\mu(k_T, p_{1,T}) = \frac{1}{p_{1,T}^2} (k^2 p_{1,T} - p_{1,T}^2 k_T); \quad \Gamma_\nu(k_T - p_{1,T}, p_{2,T}) = \frac{1}{p_{2,T}^2} ((k - p_{1,T})^2 p_{2,T} - p_{2,T}^2 (k_T - p_{1,T})); \quad (\text{B3})$$

We need to convolute these vertices with  $\Gamma_\mu(l_T, \mathbf{p}_{1,T})$  and  $\Gamma_\nu(l_T - \mathbf{p}_{1,T}, \mathbf{p}_{2,T})$  for the different Pomerons, where the integration is over  $l_T$ . In such convolution the terms that are proportional to  $\mathbf{p}_{1,T} \cdot \mathbf{k}_T$  or to  $\mathbf{p}_{1,T} \cdot l_T$  vanish due to angular integrations. Only the term which is proportional to  $(\mathbf{k}_T \cdot l_T)^2$  survives and yields  $\frac{1}{2} l_T^2 k_T^2$ . It is easy to see that this term is the same in both vertices of Eq. (B1) and Eq. (B2). Now we need to compare

$$\Gamma_\mu(\mathbf{k}_T, \mathbf{p}_T) \cdot \mathbf{p}_T = \frac{1}{p_T^2} (k^2 \mathbf{p}_T - p_T^2 \mathbf{k}_T) \cdot \mathbf{p}_T \quad (\text{B4})$$

with

$$\Gamma_\nu(\mathbf{k}_T - \mathbf{p}_T, \mathbf{p}_T) = \frac{1}{p_T^2} ((\mathbf{k} - \mathbf{p}_T)^2 \mathbf{p}_T + p_T^2 (\mathbf{k}_T - \mathbf{p}_T)) \cdot \mathbf{p}_T; \quad (\text{B5})$$

where we denote  $\mathbf{p}_{1,T} = \mathbf{p}_T = -\mathbf{p}_{2,T}$ .

The direct calculations gives the same expression for both terms:

$$\frac{1}{2} p_T^2 ((\mathbf{k}_T - \mathbf{p}_T)^2 + k_T^2 - p_T^2) \quad (\text{B6})$$

Therefore, both diagrams give the same contribution.

---

\* Electronic address: gotsman@post.tau.ac.il

† Electronic address: leving@post.tau.ac.il, eugeniy.levin@usm.cl

- [1] V. Khachatryan *et al.* [CMS Collaboration], arXiv:1510.03068 [nucl-ex]; JHEP **1009** (2010) 091 [arXiv:1009.4122 [hep-ex]]. arXiv:1510.03068 [nucl-ex].
- [2] J. Adams *et al.* [STAR Collaboration], Phys. Rev. Lett. **95** (2005) 152301 [nucl-ex/0501016].
- [3] B. Alver *et al.* [PHOBOS Collaboration], Phys. Rev. Lett. **104** (2010) 062301 [arXiv:0903.2811 [nucl-ex]].
- [4] H. Agakishiev *et al.* [STAR Collaboration], arXiv:1010.0690 [nucl-ex].
- [5] S. Chatrchyan *et al.* [CMS Collaboration], Phys. Lett. B **718** (2013) 795 [arXiv:1210.5482 [nucl-ex]]; V. Khachatryan *et al.* [CMS Collaboration], JHEP **1009** (2010) 091, [arXiv:1009.4122 [hep-ex]].
- [6] S. Chatrchyan *et al.* [CMS Collaboration], JHEP **1402** (2014) 088, [arXiv:1312.1845 [nucl-ex]]; Phys. Rev. C **89** (2014) no.4, 044906; [arXiv:1310.8651 [nucl-ex]]; “Centrality dependence of dihadron correlations and azimuthal anisotropy harmonics in PbPb collisions at  $\sqrt{s_{NN}} = 2.76$  TeV,” Eur. Phys. J. C **72** (2012) 2012 [arXiv:1201.3158 [nucl-ex]]; JHEP **1402** (2014) 088 doi:10.1007/JHEP02(2014)088 [arXiv:1312.1845 [nucl-ex]].
- [7] J. Adam *et al.* [ALICE Collaboration], arXiv:1604.07663 [nucl-ex]; Phys. Rev. Lett. **116** (2016) no.13, 132302, [arXiv:1602.01119 [nucl-ex]]; L. Milano [ALICE Collaboration], Nucl. Phys. A **931** (2014) 1017, [arXiv:1407.5808 [hep-ex]]; Y. Zhou [ALICE Collaboration], J. Phys. Conf. Ser. **509** (2014) 012029, [arXiv:1309.3237 [nucl-ex]].
- [8] B. B. Abelev *et al.* [ALICE Collaboration], Phys. Rev. C **90** (2014) no.5, 054901, [arXiv:1406.2474 [nucl-ex]]; B. B. Abelev *et al.* [ALICE Collaboration], Phys. Lett. B **726** (2013) 164 doi:10.1016/j.physletb.2013.08.024 [arXiv:1307.3237 [nucl-ex]]; B. Abelev *et al.* [ALICE Collaboration], Phys. Lett. B **719** (2013) 29, [arXiv:1212.2001 [nucl-ex]].
- [9] G. Aad *et al.* [ATLAS Collaboration], Phys. Rev. Lett. **116** (2016) 172301, [arXiv:1509.04776 [hep-ex]].
- [10] G. Aad *et al.* [ATLAS Collaboration], Phys. Rev. C **90** (2014) no.4, 044906; [arXiv:1409.1792 [hep-ex]]; B. Wosiek [ATLAS Collaboration], Annals Phys. **352** (2015) 117; G. Aad *et al.* [ATLAS Collaboration], Phys. Lett. B **725** (2013) 60, [arXiv:1303.2084 [hep-ex]].
- [11] B. Wosiek [ATLAS Collaboration], Phys. Rev. C **86** (2012) 014907, [arXiv:1203.3087 [hep-ex]].
- [12] E. M. Levin, M. G. Ryskin and S. I. Troian, Sov. J. Nucl. Phys. **23** (1976) 222 [Yad. Fiz. **23** (1976) 423]; A. Capella, A. Krzywicki and E. M. Levin, Phys. Rev. D **44** (1991) 704.
- [13] E. Gotsman, E. Levin and U. Maor, Phys. Rev. D **95**, no. 3, 034005 (2017) doi:10.1103/PhysRevD.95.034005 [arXiv:1604.04461 [hep-ph]].
- [14] A. Kovner and M. Lublinsky, Phys. Rev. D **83**, 034017 (2011), [arXiv:1012.3398 [hep-ph]].
- [15] Y. V. Kovchegov and D. E. Wertepny, Nucl. Phys. A **906** (2013) 50, [arXiv:1212.1195 [hep-ph]].
- [16] T. Altinoluk, N. Armesto, G. Beuf, A. Kovner and M. Lublinsky, Phys. Lett. B **752** (2016) 113, [arXiv:1509.03223 [hep-ph]]; T. Altinoluk, N. Armesto, G. Beuf, A. Kovner and M. Lublinsky, Phys. Lett. B **751** (2015) 448, [arXiv:1503.07126 [hep-ph]].
- [17] E. Gotsman and E. Levin, Phys. Rev. D **95** (2017) no.1, 014034 [arXiv:1611.01653 [hep-ph]].
- [18] A. Kovner, M. Lublinsky and V. Skokov, “Exploring correlations in the CGC wave function: odd azimuthal anisotropy,” arXiv:1612.07790 [hep-ph].
- [19] K. Dusling and R. Venugopalan, Phys. Rev. D **87** (2013) no.9, 094034, [arXiv:1302.7018 [hep-ph]] and reference therein.
- [20] A. Kovner and M. Lublinsky, Int. J. Mod. Phys. E **22**, 1330001 (2013), [arXiv:1211.1928 [hep-ph]] and references therein.
- [21] E. Gotsman, E. Levin and U. Maor, Eur. Phys. J. C **76** (2016) no.11, 607, arXiv:1607.00594 [hep-ph].

- [22] A. Dumitru, D. E. Kharzeev, E. M. Levin and Y. Nara, Phys. Rev. C **85** (2012) 044920, [arXiv:1111.3031 [hep-ph]].
- [23] D. Kharzeev, E. Levin and M. Nardi, Nucl. Phys. A **747**, 609 (2005), [hep-ph/0408050].
- [24] D. Kharzeev, E. Levin and M. Nardi, Nucl. Phys. A **730**, 448 (2004) Erratum: [Nucl. Phys. A **743**, 329 (2004)], [hep-ph/0212316].
- [25] D. Kharzeev, E. Levin and M. Nardi, Phys. Rev. C **71**, 054903 (2005), [hep-ph/0111315].
- [26] D. Kharzeev, E. Levin and L. McLerran, Phys. Lett. B **561**, 93 (2003), [hep-ph/0210332].
- [27] D. Kharzeev and E. Levin, Phys. Lett. B **523**, 79 (2001), [nucl-th/0108006].
- [28] D. Kharzeev and M. Nardi, Phys. Lett. B **507**, 121 (2001) doi:10.1016/S0370-2693(01)00457-9 [nucl-th/0012025].
- [29] R. Hanbury Brown and R. Q. Twiss, Nature **178** (1956) 1046.
- [30] G. Goldhaber, W. B. Fowler, S. Goldhaber and T. F. Hoang, Phys. Rev. Lett. **3**, 181 (1959); G. I. Kopylov and M. I. Podgoretsky, Sov. J. Nucl. Phys. **15**, 219 (1972) [Yad. Fiz. **15**, 392 (1972)]; G. Alexander, Rept. Prog. Phys. **66** (2003) 481, [hep-ph/0302130].
- [31] Yuri V Kovchegov and Eugene Levin, “*Quantum Chromodynamics at High Energies*”, Cambridge Monographs on Particle Physics, Nuclear Physics and Cosmology, Cambridge University Press, 2012 .
- [32] V. A. Abramovsky, V. N. Gribov and O. V. Kancheli, Yad. Fiz. **18**, 595 (1973) [Sov. J. Nucl. Phys. **18**, 308 (1974)].
- [33] L. V. Gribov, E. M. Levin and M. G. Ryskin, Phys. Rep. **100** (1983) 1.
- [34] E. M. Levin and M. G. Ryskin, Phys. Rept. **189**, 267 (1990).
- [35] A. H. Mueller, Phys. Rev. **D2** (1970) 2963.
- [36] E. A. Kuraev, L. N. Lipatov, and F. S. Fadin, Sov. Phys. JETP **45**, 199 (1977); Ya. Ya. Balitsky and L. N. Lipatov, Sov. J. Nucl. Phys. **28**, 22 (1978).
- [37] L. N. Lipatov, Phys. Rep. **286** (1997) 131; Sov. Phys. JETP **63** (1986) 904 and references therein.
- [38] E. M. Levin and M. G. Ryskin, Yad. Fiz. **25**, 849 (1977); hep-ph/9710546.
- [39] J. Bartels and M. G. Ryskin, Z. Phys. C **76**, 241 (1997), [hep-ph/9612226].
- [40] Y. V. Kovchegov, Phys. Rev. D **64**, 114016 (2001) [Erratum-ibid. D **68**, 039901 (2003)] [arXiv:hep-ph/0107256].
- [41] Y. V. Kovchegov and K. Tuchin, Phys. Rev. D **65**, 074026 (2002) [arXiv:hep-ph/0111362].
- [42] J. Jalilian-Marian and Y. V. Kovchegov, Phys. Rev. D **70**, 114017 (2004) [Erratum-ibid. D **71**, 079901 (2005)] [arXiv:hep-ph/0405266].
- [43] M. A. Braun, Eur. Phys. J. C **48**, 501 (2006) [arXiv:hep-ph/0603060].
- [44] C. Marquet, Nucl. Phys. B **705**, 319 (2005) [arXiv:hep-ph/0409023].
- [45] A. Kovner and M. Lublinsky, JHEP **0611**, 083 (2006) [arXiv:hep-ph/0609227].
- [46] E. Levin and A. Prygarin, Phys. Rev. C **78**, 065202 (2008), [arXiv:0804.4747 [hep-ph]].
- [47] J. Jalilian-Marian and Y. V. Kovchegov, Phys. Rev. D **70**, 114017 (2004) [Erratum-ibid. D **71**, 079901 (2005), [arXiv:hep-ph/0405266].
- [48] Y. L. Dokshitzer, D. Diakonov and S. I. Troian, Phys. Rept. **58** (1980) 269.
- [49] V. A. Khoze, A. D. Martin and M. G. Ryskin, Eur. Phys. J. C **48** (2006) 467 doi:10.1140/epjc/s10052-006-0025-5 [hep-ph/0605113], Eur. Phys. J. C **14** (2000) 525 doi:10.1007/s100520000359 [hep-ph/0002072]. Phys. Rev. D **56** (1997) 5867 [hep-ph/9705258]; Phys. Lett. B **401**, 330 (1997) [hep-ph/9701419].
- [50] Y. V. Kovchegov and K. Tuchin, Phys. Rev. D **65** (2002) 074026 doi:10.1103/PhysRevD.65.074026 [hep-ph/0111362].
- [51] A. H. Mueller and D. N. Triantafyllopoulos, Nucl. Phys. B **640**, 331 (2002); [hep-ph/0205167]. D. N. Triantafyllopoulos, Nucl. Phys. B **648**, 293 (2003) [hep-ph/0209121].
- [52] H. Abramowicz *et al.* [ZEUS Collaboration], Phys. Rev. D **93** (2016) no.9, 092002, [arXiv:1603.09628 [hep-ex]]; H. Abramowicz *et al.* [H1 and ZEUS Collaborations], Eur. Phys. J. C **75** (2015) no.12, 580, [arXiv:1506.06042 [hep-ex]].
- [53] V.N. Gribov and L.N. Lipatov: Sov. J. Nucl. Phys. **15** (1972) 438;  
L.N. Lipatov: Yad. Fiz. **20** (1974) 181;  
G. Altarelli and G. Parisi: Nucl. Phys. **B126** (1977) 298;  
Yu.L. Dokshitzer: Sov. Phys. JETP **46** (1977) 641.
- [54] J. L. Albacete, N. Armesto, J. G. Milhano, P. Quiroga-Arias and C. A. Salgado, Eur. Phys. J. C **71** (2011) 1705, [arXiv:1012.4408 [hep-ph]].
- [55] E. Iancu, J. D. Madrigal, A. H. Mueller, G. Soyez and D. N. Triantafyllopoulos, Phys. Lett. B **750** (2015) 643, [arXiv:1507.03651 [hep-ph]].
- [56] G. Aad *et al.* [ATLAS Collaboration], Phys. Rev. Lett. **116**, no. 17, 172301 (2016), [arXiv:1509.04776 [hep-ex]].
- [57] R.J. Glauber, In: Lectures in Theor. Phys., v. 1, ed. W.E. Brittin and L.G. Duham. NY: Intersciences, 1959
- [58] J. Bartels, J.Phys. **G19** (1993) 1611.
- [59] V. N. Gribov, Sov. Phys. JETP **26** (1967) 414 [Zh. Eksp. Teor. Fiz. **53** (1967) 654].
- [60] J. Bartels and E. Levin, Nucl. Phys. **B387** (1992) 617, E. Iancu, K. Itakura and L. McLerran, Nucl. Phys. **A708** (2002) 327 [arXiv:hep-ph/0203137].
- [61] M. Froissart, Phys. Rev. **123** (1961) 1053;  
A. Martin, “*Scattering Theory: Unitarity, Analyticity and Crossing.*” Lecture Notes in Physics, Springer-Verlag, Berlin-Heidelberg-New-York, 1969.